

Consortium



for

Small-Scale Modelling

Newsletter

May 2022

No.21

Ufficio Generale Spazio Aereo e
Meteorologia

Institut Meteorologii i Gospodarki
Wodnej

Federal Service for Hydrometeorology
and Environmental Monitoring

Centro Italiano Ricerche Aerospaziali

Amt für GeoInformationswesen der
Bundeswehr

CIMA Foundation

ΕΘΝΙΚΗ ΜΕΤΕΩΡΟΛΟΓΙΚΗ
ΥΠΗΡΕΣΙΑ

Administratia Nationala de
Meteorologie

Agenzia Regionale per la Protezione
Ambientale dell'Emilia Romagna
Servizio Idro Meteo Clima

Israel Meteorological Service

Agenzia Regionale per la Protezione
Ambientale del Piemonte

Centro euro-Mediterraneo sui
Cambiamenti Climatici

www.cosmo-model.org

Editor: Mihaela Bogdan (NMA)

The CC license "BY-NC-ND" allows others only to download the publication and share it with others as long as they credit the publication, but they can't change it in any way or use it commercially.



Publisher

Editor

COSMO
Consortium for Small Scale Modelling
cosmo-model.org

Mihaela Bogdan, NMA
mihaela.bogdan@meteoromania.ro

Contributions to COSMO Newsletter No. 21 have DOIs.
These are indicated on the title page of each contribution.
The DOI format is 10.5676/dwd_pub/nwv/cosmo-nl_21_NN, where NN is the contribution number.

Table of Contents

1 Editorial	1
<i>Gebhardt Christoph</i>	1
2 Working Group on Data Assimilation	3
Derecho of 11 August 2017 confirms the Thunderstorm Thermometer approach <i>Jan Parfiniewicz</i>	3
Briefly about the derecho event over Poland in 11 August 2017 <i>Jan Parfiniewicz, Piotr Barański, Wojciech Gajda, Jerzy Konarski, Witold Interewicz, Wiesław Lazarewicz, Jan Walasek</i>	15
3 Working Group on Verification and Case Studies	21
Summary of Results from the COSMO Priority Project CARMA: Common Area with Rfd-bk/MEC Application <i>A. Iriza-Burcă, F. Gofa, D. Boucouwala, T. Andreadis, J. Linkowska, P. Khain, A. Shtivelman, F. Batignani, A. Pauling, A. Kirsanov, T. Gastaldo, B. Maco, M. Bogdan, F. Fundel</i>	21
Common Area Results 2020-2021 <i>Flora Gofa</i>	28
4 Working Group on Implementation and Reference Version	39
COSMO-Model 6.0 - The Last Official Version <i>Ulrich Schättler</i>	39
5 Mission Reports	45
Priority Project COSMO-EULAG Operationalization (PP CELO) <i>Bogdan Rosa, Marcin J. Kurowski, Joanna Linkowska, Zbigniew P. Piotrowski, Damian K. Wójcik and Michał Z. Ziemiański</i>	45
Priority Task Consolidation of COSMO-EULAG (PT CCE) <i>Damian K. Wójcik, Bogdan Rosa and Michał Z. Ziemiański</i>	50
Appendix: List of COSMO Newsletters and Technical Reports	55

The transition from the limited-area model COSMO to the limited area mode of the ICON modelling framework (ICON-LAM) within the Consortium for Small-Scale modelling has made considerable progress during the recent years. All COSMO member states are now prepared and able to run a deterministic forecast with ICON-LAM on a regular basis. The considerable achievements by the COSMO priority project C2I were essential to reach this milestone. The consortium is deeply grateful to all contributors to the PP C2I and the project leader Daniel Rieger (DWD) for their effort and support. With PP C2I coming to its end in spring 2022, the consortium is now in a good position to pursue further steps of the transition in terms of implementation to operations and scientific development within its Working Groups and dedicated priority projects and tasks. In fact, this work has already started in Priority Projects like CITTA ("City Induced Temperature change Through Advanced modelling", started in 07/21) aiming at the transition of the achievements of PT AEVUS & AEVUS2 to ICON. Moreover, the Priority Project CAIR ("Clouds and Aerosols Improvements in ICON Radiation Scheme") continues with relevant improvements in ICON in its second phase PP CAIR-2 (started in 03/22). Another example is the sensitivity study on ICON model parameters presented at ICCARUS 2022 by E. Avgoustoglou and colleagues from four COSMO partners. However, there are further steps to go towards the transition to ICON, which will require some efforts and will pose challenges as well. The COSMO and ICON communities will have to liaise closer in future, concerning scientific and technical aspects as well as organizational structures and administrative procedures. The process of defining suitable agreements and pathways for an effective and beneficial cooperation and the indispensable exchange of information is ongoing on various levels. One of the next steps in this direction will be the joint session of the Scientific Management Committee and members of the ICON community during the ICON All Staff Meeting in June 2022.

The transition to ICON has consequences for generating revenue in COSMO from license fees, which in turn are used to fund COSMO activity proposals. While COSMO license fees are currently paid for the operational use of the COSMO model, this is not analogously applicable to the operational use of ICON. However, the consortium strives towards providing support for ICON users under a license with annual fees. This support has to be established within COSMO and a first preparatory step is the new PP ICON-COMFORT ("ICON-competence in forecasting", started in 03/22).

When new prospects emerge, some familiar and well-established basics start to stand back. On 14th December 2021, COSMO 6.0 has been released as the final official version of the COSMO model. This model has been the scientific core of the consortium for many years providing a sense of common identity for the COSMO partners. A dedicated contribution of the SCA Uli Schättler (DWD) about COSMO 6.0 in this COSMO newsletter emphasizes the importance of the COSMO model for our community.

Since the release of COSMO Newsletter No. 20, further priority projects and tasks were completed with success: PT SAINT ("Snow cover Atmosphere Interactions"), PP AWARE ("Appraisal of 'Challenging Weather' forecasts"), and PP CARMA ("Common Area with Rfdbk/Mec Application"). PP CARMA resulted in a restructured procedure for common plot activities and has been the basis for the implementation of a very useful shiny application for the interactive generation of verification plots (see <https://www.cosmo-model.org/content/tasks/verification.priv/default.htm>). There is a contribution about PP CARMA in this issue of the COSMO Newsletter by the project leader Amalia Iriza-Burca (NMA) and the PP CARMA team.

The COVID-19 pandemic prevented us from having in-person meetings in 2021. Not only smaller meetings of STC, SMC or working groups were held online, but also the COSMO General Meeting 2021 as well as ICCARUS 2022 had to be restricted to an online event once again. Even though we can be glad to benefit from good technical infrastructure and excellent support by the staff organizing

the online meetings and even though we adopt to these circumstances more and more, there is an increasing need and desire to meet in person again after more than two years. Looking at the currently lowering numbers of COVID infections, let us keep fingers crossed that the "COSMO family" will be able to meet in Athens in September 2022, though a decision is still due.

Last, but not least, we welcome the CIMA foundation (<https://www.cimafoundation.org/>), Italy, as new participating member to COSMO.

I would like to thank all contributors to the COSMO Newsletter No. 21 and the editorial team, in particular Mihaela Bogdan and Massimo Milelli, for the effort put into setting up this issue of the Newsletter.

Looking forward to more in-person meetings,

Gebhardt Christoph
COSMO Scientific Project Manager

Derecho of 11 August 2017 confirms the Thunderstorm Thermometer approach.

JAN PARFINIEWICZ

Institute of Meteorology and Water Management - National Research Institute, Warsaw, Poland

1 Introduction

Let us refer to formulas presented on the EMS2012 meeting, Expo 2013 and confirmed in Newsletter 16 (Parfiniewicz J., 2014, Parfiniewicz J. and Konarski J., 2016) . The 1st Formula (*), the best filter for strong Tornado or Downburst events expresses Fujita scale as a square root function merely of the Intra-Cloud discharges densities, while, the 2nd (**) for less severe events takes into account both: IntraCloud and Cloud-to-ground lightning discharges densities. It has occurred, that both formulas might have clear physical interpretation. Indeed, Formulas (1) and (2) distinctly differentiate lightning activity that is characteristic for two various developing thunderstorm stages, i.e., for the mature one and the second for the dissipation thundercloud formation, In the mature, active stage IntraCloud lightning prevails, while the second is dominated by Cloud-to-ground lightning discharges.

Operational monitoring of tornados showed that extreme Tornado or Downburst events are strictly correlated to IntraCloud number of flashes aggregated in cells over approximately 15 km radius area. However working on the 7 by 7 km (or 2.8 by 2.8 km) square grid these densities are being enhanced to remain the accordance with typical supercells diameter.

Let's turn to Nowcasting and Forecasting Strong Convective Events (SCE). The 3 categories are highlighted to distinguish between Nowcast and Forecast: ,i.e., lead time, the method used, and finally the targeted product. For lead time: we have tens of hours against 1 hour, for methodology: probabilistic interpretation of the model against tendency plus probabilistic interpretation plus possibly HD accurate simulations - if occurred, and finally: danger zones against accurate location. The successful nowcasting in fact is measured in minutes (after James Anderson, EXPO2013).

What we have practiced in Poland it is the Observed Storms category which might serves merely as an introduction to Nowcasting SCE showing their possible growth or decay and helps to understand how will they propagate.

Now the issue is how to embrace this extremely strong convection process and express it within conventional Euler - Lagrange approach fluid dynamics models.

2 Recapitulation EXPO_2013 – EMS_2012

What is essential to obtain an effective thunderstorm prediction is, firstly, **to operate self-learning algorithms**, secondly, **to possess skills to quantify the strength of convection and thunderstorm severity**, and, finally, **to organize an end-user oriented warning system**.

The prediction system (lead time 36 hours) is fed by the SYNOP (code WW) data and the PERUN data. Initially, PERUN data was only used to confirm or deny the occurrence of a storm, but not to determine its strength.

doi:10.5676/dwd_pub/nwv/cosmo-nl_21_02

It turned out, however, that in cases of tornado incidents such a passive scale of storm severity is not adequate for teaching the prediction system about these extreme cases. Therefore, a hybrid scaling system was introduced by modifying WW observations with the information on the severity of storms from the SAFIR / PERUN system in accordance with the formulas (*) and (**). The SAFIR/PERUN network system provides lighting information in six categories: cloud-to-ground (CG) flashes divided into return and subsequent strokes (Rs and Ss), intracloud discharges (IC), where the emission (nodal) points of IC strokes are subdivided into (ICs)start, (ICi)intermediate and (ICe)end points and Isolated emission points (Is).

The following topics will be covered:

1. Thunderstorm quantification issue
2. Scaling Convection Strength
3. Universal to local. Optimum Interpolation / Interpretation (OI)
4. Self-learning Engine
5. Forecasting vs. Nowcasting
6. How was it practiced in Poland
7. On the way to understand stormy weather

2.1 Thunderstorm quantification issue: the **Thunderstorm Thermometer**

The review of the polish press reports and investigation of the SKYWARN POLSKA

[http : //lowcyburz.pl/](http://lowcyburz.pl/) archives, including personal contact with A. Surowiecki (the Polish Skywarn representative) led to collecting twenty dates with extreme ToD (Tornado or Downburst - ToD) events. More, A.Surowiecki has been given an eye-witness Fujita value to each event. Now, the statistics over 27887 aggregated cells, filtered in many possible ways has been constructed to fit to expected Fujita [F] values.

The best filter for strong ToD events with $[F] \geq 1$ (more or even) giving correlation $R \approx 0.85$ reads:

$$[F] = a * (b * IC_{-s} + c * IC_{-i})^{1/2} + d$$

under condition

$$Rs > 1 \& IC_{-s} > 70[NoF](*)$$

$$where : a = 0.047, b = 0.7, c = 0.3, d = 0.22 \text{ and } IC_{-s}, IC_{-i}$$

are measured in $[NoF/\pi 15km^2 \cdot 10min.]$

For less severe events with $0 < [F] \leq 2.5$ another indicator-filter which includes CG flashes (Rs_i0) is being recommended:

$$[F] = a * (b * IC_{-s} + c * Rs + d * (IC_{-s} * Rs)^{1/2})^{1/2}(**)$$

where: a=0.088, b=0.624, c=0.112, d=0.264

Thunderstorm Thermometer Formulae : lightning discharges density function.

Operational monitoring of tornados that were observed over Poland in summer season of 2012/2013 showed that extreme ToD events are strictly correlated to IC number of flashes [NoF] aggregated in cells over a 15 km radius area $[\pi \cdot 15km^2]$ (what is equivalent to significant enhancement regarding 7x7 km resolution) within 10 minute interval. PERUN's signal conversion is carried out on 7x7 and 2.8 x 2.8 grids, but for each grid node, the surroundings up to 15 km are screened. If the PERUN signal is present in this environment, the value of the discharge density in a given localization is amplified.

The relationship between virtual Fujita scale [F] and the 'classical' measurement from PERUN for selected thresholds generally depends on the grid resolution and statistics. For the COSMO_07 km reference grid in

Table 1: Relationship between [F] and PERUN measurement for selected thresholds 07km grid

IC_s	IC_i	RS	thresholds
139.	117.	78.	1.0
636.	361.	233.	2.0
1514.	1036.	347.	3.0
2652.	2073.	590.	4.0
4128.	2839.	1090.	5.0

Table 2: Relationship between VFS and PERUN measurement for selected thresholds 2.8km grid

IC_s	IC_i	RS	thresholds
68.	39.	24.	0.5
137.	93.	105.	1.0
644.	532.	175.	2.0
1499.	1092.	274.	3.0
2696.	1503.	384.	4.0
5384.	2960.	860.	5.0

10 min. intervals and data for the whole day of 11 August 2017 we have Tab. 1, for the COSMO_2.8 grid Tab. 2 :

In Sketch 1, the densities are computed on a 2.8 by 2.8 km square grid. In order to conform to the typical diameter of supercells, it is necessary to amplify the commonly used values by a factor that ranges from 0 to 36, according to a weighting function that increases with distance from the center of the square.

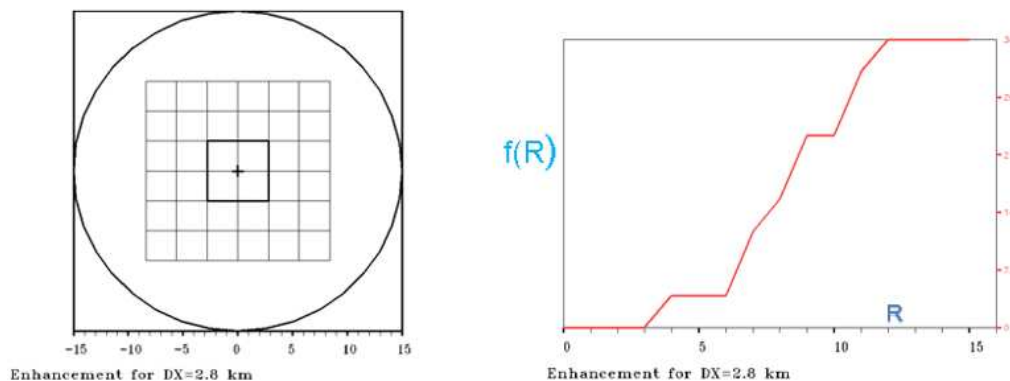


Figure 1: Sketch 1-Equivalent enhancement for 2.8 by 2.8 km square grid

Interpretation. Formulas (*) and (**) distinctly **differentiate** between specific **lightning activity** that is **characteristic for two** various developing **thunderstorm stages**, i.e., for the **mature and very active** one, **with dominant IC flash** generation and the second for **the dissipation thundercloud formation**, **when CG flash generation** is increasing and is **more pronounced**.

Expression (*) by explicit inclusion of the **IC_i** component is confirming well known fact (see e. g., Rakov and Uman, 2003) that so-called **spider lightning** with great number of branches, with the great **IC_i** are **appearing** frequently **during mature stages of supercells**. (P.Barański 2009,2012)

2.2 Scaling Convection Strength

Let's now discuss the Convective Scale (CS) which is essential to build up Self-learning Stochastic Forecasting Model. At 1st, the synop weather code was squeezed into seven-step scale of natural gradation. This seven step scale starts with No Convection and finishes with Thunderstorm with hail along with clouds development : starting with Cumulus and finishes with Cumulonimbus Capilatus. But since storm is not equal to storm, it has become necessary to extend this scale.

To build up the New CS scale we may simply add to the 7th step SYNOP scale the 5th step of Fujita scale thus obtaining twelfth step scale which covers Strong Convective Events including tornados. Now, we have seven classical steps from No Convection to Thunderstorm with hail and additional 5 steps devoted to tornados and supercells. Possibly there exists a correlation between this Convection scale and with the Beaufort scale of wind strength.

2.3 Universal to local. Optimum Interpolation / Interpretation (OI) vs Kalman Filter (KF)

Predicting storms and tornadoes with traditional hydrodynamic (HD) methods by NWP systems does not seem realistic. We propose an approach: the HD model generates a "universal" prognostic signal at the Input, and the self-learning engines provide a local stochastic response at the Output. The sum of the local responses is an estimate of the storm forecast field. In fact, the same (or a similar) idea was behind the: "WMO Symposium on the interpretation of broad-scale NWP products for local forecasting purposes" (11-16 October 1976; Warsaw, Poland). On the other hand, the problem of physic-statistical forecasting methods has a rich tradition of the Russian school, including such authoritative names as A.N.Kolmogorov, A.M.Obukhov, M.I. Yudin, A.M.Yaglom (Yaglom, 1963).

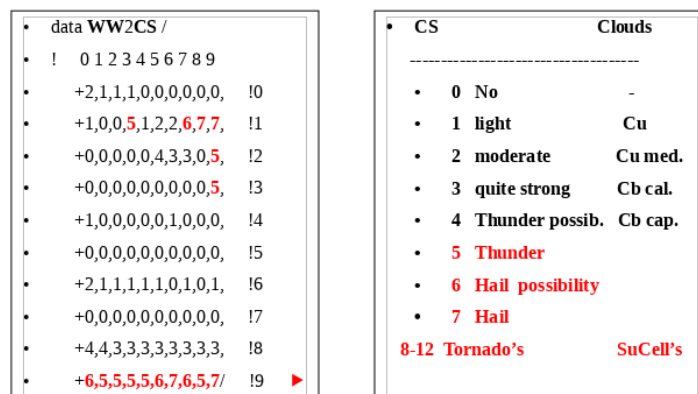


Figure 2: Sketch 2 - New CS scale = CS/WW [0-7] + [0-5] FUJITA = [0-12]

Following this path (Gandin L.S. 1963, Kagan R.L. 1966, Rukhovets L.V. 2006), a simple (but effective) method of Gandin's Optimal Interpolation was adopted to local forecasting (statistical interpretation of the NWP), replacing or even extending the functionalities obtained with the KF.

The OI formalism itself is trivial and comes down to solving a simple system of equations: $\mu\Pi = \mu0$, where Π are weights of linear regression of individual predictors, and μ , $\mu0$ are the predictors correlation matrix and the correlation vector between predictor - predictors .

The catch is that the statistical structure behind this system of correlation, dispersion and means matrices is location dependent, monitored and moderated to create a pseudo "climate" on a domain of forecast. The great advantage of OI is that each regression set has its own accuracy metric in the form of a total correlation coefficient R (see & compare Yaglom, 1963 and Gandin, 1963): $R^2 = \sum(\mu0 * \Pi)$. An important moment is also the limitation of the number of predictors to 5 (Yaglom, 1963), with the 5th being selected again from a much larger number of potential predictors (here 21).

2.4 Self-learning Engine

The physical-stochastic approach has been applied to improve ideas referred to very early,-1976, work: "The prediction of air mass thunderstorms and hails" by Lityńska , Parfiniewicz & Piwkowski. With the particularity to statistical method the method used is almost identical to Collins & Tissot (CT), 2007 ([http : //lighthouse.tamucc.edu/dnrpub/nn - channel - 3.wmv](http://lighthouse.tamucc.edu/dnrpub/nn-channel-3.wmv)). Here the OI - i.e. self-learning statistical structure (generalised to automatic renewal of the new multi-regression set of parameters), there - self learning Artificial Neural Net. The genesis of these two works is quite independent, however from the CT the idea of the ROC curves has been adopted to reverse continues (quantitative) probabilistic input signal onto qualitative [0,1] output. The actual proposition recapitulate the earlier authors searches concerning Tornado prediction, (Parfiniewicz et all, 2011), from which clearly indicates that the current NWP models would not be able to predict strong convection events in frame of pure hydro-dynamical approach.

The algorithm is learning of "good forecasting" basing on meteorological stations (observations by SYNOP WW key) and lightning activity detected by the SAFIR/PERUN network system, all restored every 1h. The "universal" forecasting signal is generated by COSMO-7km (2.8km) model and the local stochastic response is then taken every 1h on each grid network via interpolation from neighbouring stations statistical characteristic (called "modified climate"). To forecast thunderstorm (convectivness) the 21 predictors (the physical parameters calculated from COSMO model) has been chosen. They might be gathered into 5 categories that describe the state of the atmosphere via: humidity (the several indexes), available convective (instability) energy (the several indexes, including CAPE derivatives), the stratification of the atmosphere (including the heights of the isotherm 0 C and -20 C), the synoptic background (vorticity, pressure tendency, vertical velocity). These 21 potential parameters guarantee that the maximum part of thunderstorm dispersion was described for each of 57 synoptic stations separately (an example Tab.1).

From these 21 potentially available indexes every 1h the set of 5 is automatically renewed (what means some generalisation). Parallel to predictability of the thunderstorm the Strength of Convection in the 0-7 scale (from absence to thunderstorm with hail) is being taken basing on the WW SNOB key. The predictions in form maps and diagrams was tested on the IMGW aviation portal. The currently calculated POD and FAR indicators are relatively high (0.6-0.8, 0.2-0.4) depending on the station the correlation (1point/1h) is about 0.5 but for time/space surroundings much higher.

Kasprowy_Wierch			Ustka		ALL	
k	name	R	name	R	name	R
1	Q850	0.585	vLEVclc	0.606	Wlt_T_Td	0.506
2	Sumaqcqv	0.631	P0_MODEL	0.657	PLNB_CTH	0.566
3	z20	0.659	z20	0.677	vLEVclc	0.587
4	PLNB_CTH	0.672	PLNB_CBH	0.683	z20	0.599
5	vLEVqc	0.684	DP0_MODEL	0.691	vLEVqcqv	0.608
6	P0_MODEL	0.694	Qsrf1E3_MO	0.697	CINS	0.613
7	CINS	0.696	slin	0.699	DP0_MODEL	0.616
8	slin	0.696	CINS	0.701	Wmin	0.620
9	Qsrf1E3_MO	0.699	Wlt_T_Td	0.703	P0_MODEL	0.623
10	Wmin	0.700	HLNB_CBH	0.704	zt0_20mx	0.624
11	vLEVclc	0.700	Wmax	0.706	Q850	0.625
12	vLEVqcqv	0.700	Sumaqv	0.707	RRRmm_24_M	0.626
13	DP0_MODEL	0.700	RRRmm_24_M	0.708	PLNB_CBH	0.626
14	RRRmm_24_M	0.700	Q850	0.709	HLCL	0.626
15	HLCL	0.701	HLCL	0.714	Sumaqcqv	0.629
16	zt0_20mx	0.701	vLEVqc	0.714	vLEVqc	0.629
17	PLNB_CBH	0.701	Wmin	0.714	slin	0.630
18	HLNB_CBH	0.701	PLNB_CTH	0.716	Wmax	0.630
19	Wlt_T_Td	0.701	zt0_20mx	0.716	Qsrf1E3_MO	0.630
20	Wmax	0.701	vLEVqcqv	0.716	Sumaqv	0.630
21	Sumaqv	0.701	Sumaqcqv	0.716	HLNB_CBH	0.630

Table 3: An example of finding the optimal set of predictors for storm prediction [0/1] for mountain's (Kasprowy Wierch), marine's (Ustka) and all regions.

nicknames	description of predictors
P0_MODEL	Surface pressure [Pa]
Qsrf1E3_MO	Surface specific humidity
RRRmm_24_M	Model rainfall for the last hour in [mm/24h]
DP0_MODEL	Surface pressure tendency [Pa]
CINS	CIN [J/KG] Convective inhibition energy
HLCL	Height OF LCL [m] - Lifting Condensation Level
HLNB_CBH	Height of lowest EQUILIBRIUM Level (Takahashi,2012)
PLNB_CBH	Pressure of lowest EQUILIBRIUM Level (Takahashi,2012)
slin	Showalter Index - measure of thunderstorm severity
PLNB_CTH	Pressure of highest EQUILIBRIUM Level (Takahashi,2012)
Wmax	Max. vertical speed in the profile
Wmin	Min. vertical speed in the profile
z20	Height of the isotherm $T = -20C$
Q850	Specific humidity at 850 hPa
vLEVqc	Specific cloud water content [kg/kg] above isotherm 0
vLEVqcqv	QC&QV [kg/kg] (cloud water & humidity)above isot.0
vLEVclc	Sum of CLC (% of Cloud Cover) in the profile
zt0_20mx	Height difference: $H(T: -20C) - H(T: 0C)$
Sumaqv	Sum of QV (specific humidity) in the profile
Sumaqcqv	Total sum of (humidity) qv and qc (cloud water)
Wlt_T_Td	Humidity indicator (Sum $T-Td/850,700,500hPa$; Lityńska 1976)
Storms01	Storms [0/1]

Table 4: Predictor nicknames and their description

2.5 Self-learning Engine

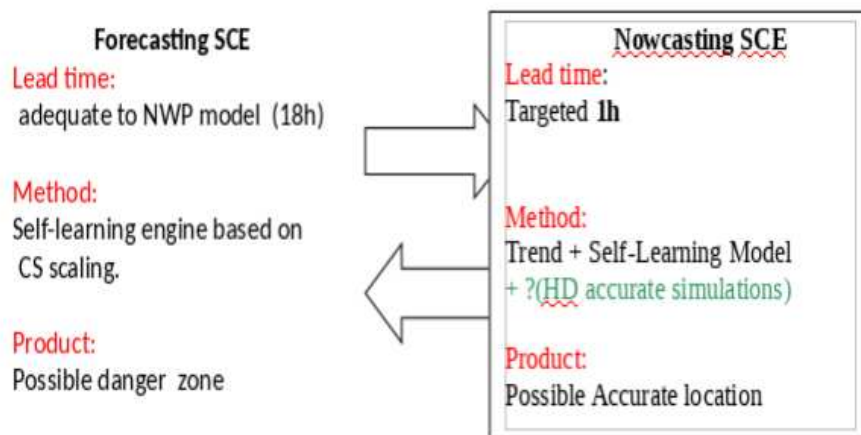


Figure 3: Sketch 3 -Forecasting and Nowcasting schemes depend on each other.

2.6 How was it practiced in Poland

1. Observed Storms category serves as an introduction to Nowcasting and it illustrates the tendency of showing possible growth or decay and movement of Strong Convective Events (SCE). This in fact ensures their monitoring - one may overlap the graph in time of self-predicted potential probabilities on it to better recognize the future position of supercell. Finally the Supercells animation helps us understand how will they propagate.
2. It is important to compare the Observed storms and Possible danger zone, just to form one's own meaning of what is the value of forecasted fields. We have also the possibility to distinguish generated forecasted fields by changing resolution model (COSMO-2.8km, 07km, 14km), and some other categories.

2.7 On the way to understand stormy weather

The way to understand stormy weather led through the study of particularly severe cases:

1st: 28 MARCH 1997 – dry stratospheric intrusion with severe storm over Poland

2end: 20th of July 2007 – explosive convection over Europe

3ed derecho 20170811

The conclusions of these cases reads as follows:

1. Explosive Convection is governed by NonHydrostatic Pressure. (seems trivial, but here the wind acceleration – is taken in the sense given by Gal-chen).
2. Despite, the assimilation of Doppler wind provide a quite realistic approximation of the tornado's, the prediction via traditional H-D methods seems unreal. (because it is rather unrealistic to retrieve accurately initial NonHydrostatic oscillations).
3. So the remedy, H-D model might generate “universal” forecasting signal but Self-learning Engines will provide the local stochastic response

28 MARCH 1997 – severe storm over Poland :”**Good Friday case**”

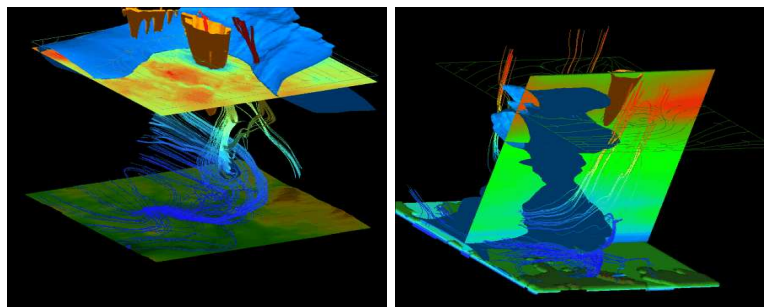


Figure 4: **Sketch 3** - Represents subsynoptic background (organization of motion) + Nonhydrostatic Pressure Fluctuations. We see the strong convergence in the lower troposphere associated with the active low pressure center, the compensating upper inflow (due to dry stratospheric intrusion) has been found near tropopause folding center with the hole in maximum velocity field of Jetstream (in brown).

20th of July 2007 – explosive convection over Europe with **severe Tornado over Poland**.

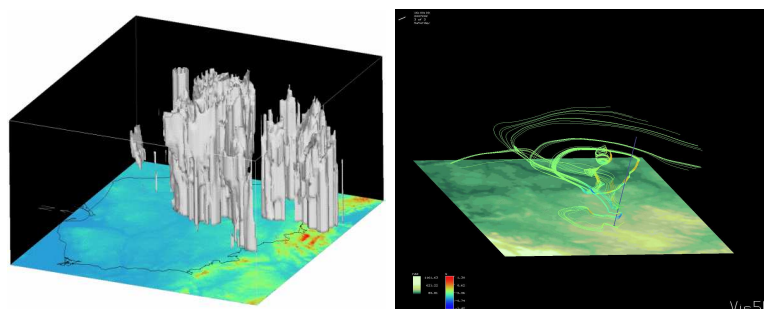


Figure 5: **Sketch 4**-Left panel: 3D composite model image of radar reflectivity- case: 20 July 2007 Right panel: Vis5d was used to obtain 3D streamlines as set of characteristic trajectories

Comment: complementing the article (Parfiniewicz, 2010) the formulas that allows on retrieving the tornado vortex are attached: “. . . retrieval of tangential wind component on polar grid circles (or part of them depending on the domain) by solving differentiated continuity equation by tridiagonal TDMA solver. The continuity equation for polar components , , reads: V_R, V_θ, V_Z .

$$\frac{\partial R * V_R}{R * \partial R} + \frac{\partial V_\theta}{R * \partial \theta} + V_Z = 0$$

Differentiating above due to θ and neglecting tangential changes V_Z reads:

$$\frac{\partial(R * \Delta\theta * \frac{\partial R * V_R}{R * \partial R})}{\partial \theta_i} = \frac{\partial^2 V_\theta}{\partial \theta_i^2}$$

where vectors of tridiagonal matrix $a(i) = 1., b(i) = -2., c(i) = 1.$ and boundary forcing values $f(0) = 0, f(Nx+1) = 0$ or $f(0) = f(Nx+1).$ “

11th of August 2017 – severe Derecho over Poland.

Figure 3 is a summary of the analysis of the derecho on August 11, 2017 that swept through Poland. The main path of the disturbance was abstracted, practically coinciding with the eastern path. In the figure it is shown as a bold purple line, superimposed on the circles (which converge into 1 serpentine line) colored according to the VFS (virtual Fujita scale) graduation for each of the 68 scans. The thin green line corresponds to the western flank and, as previous analysis showed, at least until 20:00 UTC must coincide with the main track.

This means that at that time the convective system moving over Poland was coherent in the sense of the understandable similarity of the successive images of electrical activity and - probably - the organization of motion. Between 20:00 and 21:00 UTC there was some formation of a separate storm focus in the Suszek area, which would retain its subjectivity (coherence) in the northward movement. This is a creation, detachment or split (whatever we call it), and the green line detached from the main track is a side path of the derecho disturbance. The picture shows 24 telemetric measurements of gusts exceeding 20 m/s.

Although these characteristic values on both sides of the main track, wind activity seems to prevail on the west side and correlates with the most spectacular casualties and damage, e.g. in Bory Tucholskie, while in its eastern part prevailed the electric activity of the derecho. The western flank is also better documented with radar data from Poznań and Gdańsk.

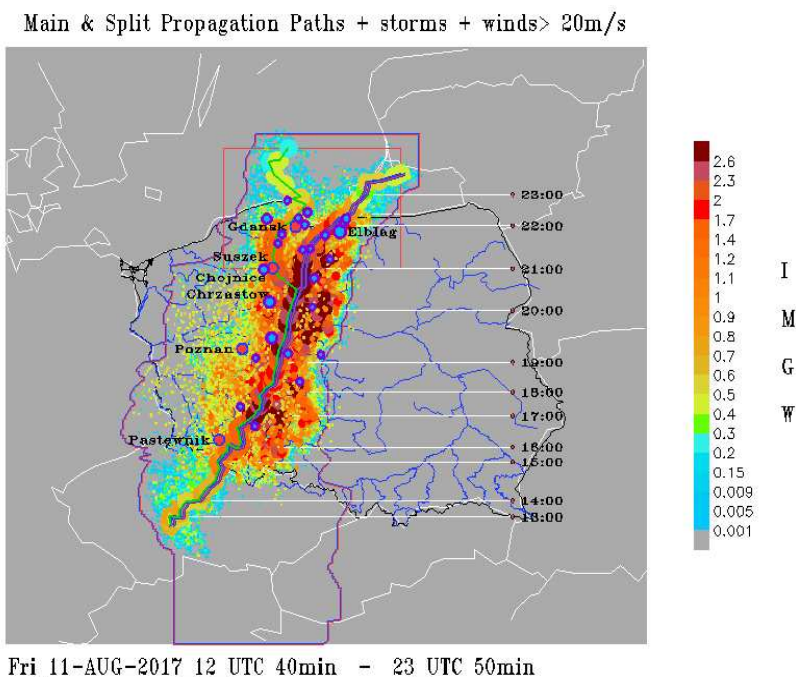


Figure 6: Main /Right & Left Propagation Paths + storms + winds \geq 20 m/s. (\circ). Winds \geq 20 m/s (in blue and violet) and circle sizes are proportional to wind strength.

According to Fig. 3. the main path of propagation is expressed in the coordinates of the COSMO_2.8 model and was used to determine the velocity. The speed is based on the position of the system + -10 minutes in relation to the moment. The highest estimated speeds (up to 40 m/s) occurred around 19:30 UTC, preceding the split stage.

Note that the estimation of the propagation speed of the western track during the division period (20:00 - 21:00 UTC) is possibly distorted by a significant error. The basic characteristics of the derecho were estimated: distance, time and average speed. And so: the total distance - 864.42 km, covered in 11.17 hours, with an average speed of 21.50 m/s (77.4 km/h).

3. Conclusions remarks

As it was pointed above the issue is to embrace the whole convection process and express it via fluid dynamics methods. Usually we use one of number convection parameterizations algorithms which allows on convective precipitation prediction giving latent heat feed back to the model. Convective precipitation is directly related to radar reflectivity (eg. via Marshall – Palmer formula). What if we merge convective precipitation with thunderstorms using lightning discharges density function.

Finally we will have referencing reflectivity with numbers beneath 55 dBz as real, and numbers above 55 (till presume 110) artificially representing this convection strength which is related to Fujita scale. This referencing reflectivity might be treated by conventional fluid dynamics models as continuum scalar value allowing on it propagation and evolution.

Acknolegmets

To Piotr Barański, Wiesław Lazarewicz,...

References

- [1] Barański P. and Parfniewicz J., 2019: The derecho episode in the Bory Tucholskie district 11 August 2017 – the present state of the predicting severe storms by awiacja_imgw_pl, ECSS2019-6-2, 4–8 November 2019, Kraków, Poland. <https://doi.org/10.13140/RG.2.2.19737.36965>
- [2] Parfniewicz J. and Konarski J., 2016: On thunderstorm quantification (continuation), COSMO Newsletter No. 16,13,14 , <https://doi.org/10.13140/rg.2.2.29118.08007>
- [3] Parfniewicz J. and Barański P., 2014: An Explosive Convection over Europe with 8-Minute tornado incident in Poland on July 20, 2007, Int. J. Environ. Eng. Nat. Resour., vol. 1, No. 6, pp. **262-276**.
- [4] Anderson J., 2013, Generating intelligent weather forecasts and advanced alerting with real-time observations, Meteorological Technology World Expo 2013, Brussels, Belgium, 15 -17 oct.
- [5] Parfniewicz J., 2013, On thunderstorm quantification, COSMO Newsletter No. 13, April 2013 (<http://www.cosmo-model.org/content/model/documentation/newsLetters>)
- [6] Parfniewicz J., 2012: Concerning Thunderstorm Potential prediction. The European Meteorological Society Annual Meeting and 9th European Conference on Applied Climatology, Łódź, Poland, 10-15 September 2012. Abstracts vol. 9, EMS2012-81. <http://meetingorganizer.copernicus.org/EMS2012/EMS2012-81.pdf>
- [7] Jan Parfniewicz, February 2011 . 20th of July 2007 tornado – towards prediction. Newsletter No. 11, www.cosmo-model.org, 3 Working Group on Verification and Case Studies pp. **82-88**
- [8] Parfniewicz J., 2010: Retrieving tornado's like wind structure (20.07.2007, Czestochowa, Poland case) using singular radar Doppler velocity , 5 Working Group on Verification and Case Studies, COSMO Newsletter 10 , pp. **70 –71**
- [9] Parfniewicz Jan, Piotr Barański, and Wojciech Gajda, 2009 , Preliminary Analysis of Dynamic Evolution and Lightning Activity Associated with Supercell Event: Case Story of the Severe Storm with Tornado and Two Heavy Hail Gushes in Poland on 20 July 2007, Publs. Inst. Geophys. Pol. Acad. Sc., D-73 (412), 2009, p. **65 – 88**
- [10] Jan Parfniewicz, 2009 20th of July 2007 – explosive convection over Europe. The COSMO perspective. IMGW, COSMO Newsletter No.9, p. **79 - 85**. Working Group on Verification and Case Studies, <http://www.cosmomodel.org/content/model/documentation/newsLetters/newsLetter09/>
- [11] Collins W. and P. Tissot, 2007: Use of an artificial neural network to forecast thunderstorm location: performance enhancement attempt. 22nd Conference on Weather Analysis and Forecasting/18th Conference on Numerical Weather Prediction; available also by the link to: <http://ams.confex.com/ams/pdfpapers/132577.pdf> and <http://ams.confex.com/ams/22WAF18NWP/techprogram/programexpanded414.htm>
- [12] Rakov, V.A., and M.A. Uman, 2003: Chap. 9, 326. In: Lightning: Physics and Effects, Cambridge University Press, Cambridge, U.K.

- [13] Parfiniewicz J., 2001, Addendum to „ Diagnostic study – storm over Poland”. Meteorologische Zeitschrift, Vol.10. No2, pp.**901-902**, <https://doi.org/10.1127/0941-2948/2001/0010-0151>
- [14] Parfiniewicz J.W., 2000 : Diagnostic study of the severe storm over Poland on 28 march 1997 - a fine mesh retrieval perspective . „Meteorologische Zeitschrift ”, Vol.9, No 5. **247- 256** (October 2000)
- [15] Parfiniewicz, J.W.; 1999, Rapid cyclogenesis over Poland on 28 March 1997. Meteorol. Appl. 6, **363-370**
- [16] Parfiniewicz J.W., 1999, On the simple retrieval algorithms adopted to study the severe storm case over Poland on 28 march 1997, Third International SRNWP- Workshop on Nonhydrostatic Modeling, Offenbach 25- 27 Oct. 1999.
- [17] Parfiniewicz J., 1998, Diagnostic study of severe Storm over Poland on 28 March 1997, Sec. Study Conf. on BALTEX, Rugen,Germany 25- 29 May 1998, Conf.Proc., Int.Secr.Publ. No 11, **168- 130**
- [18] Litynska Z, Parfiniewicz J. , Piwkowski H., 1976, The prediction of air mass thunderstorms and hails. WMO symposium on the interpretation of the broad scale NWP products for local forecasting purposes. WMO 450 , **128-130**
- [19] Parfiniewicz J., 1969. The role of convection in the hail formation process. MSc thesis. WTU
- [20] Gandin L.S. Objective analysis of meteorological fields. L. : Gidrometeoizdat, 1963, 287 p.,(in Russian).
- [21] P. L. Kagan, P. P. Drozdovskaya. On the interpolation of meteorological elements in time // Proceedings of the GGO, 1966, no. 194, .,(in Russian).
- [22] Yaglom A.M. Statistical methods of extrapolation of meteorological fields // Proceedings of the Scientific Meteorological Meeting, vol. 2. Leningrad: Gidrometeoizdat, 1963, p.**221-234**,.(in Russian).
- [23] L.V. Rukhovets, A posteriori correction of variances of forecast and observation errors December 2006, Izvestiya Atmospheric and Oceanic Physics 42 (6): 785-790 DOI: 10.1134 / S0001433806060132 ,(in Russian).
- [24] Takahashi, Hanii; Z. Luo, 2012. ”Where is the level of neutral buoyancy for deep convection?”. Geophys. Res. Lett. 39 (L15809), Volume39, Issue15. doi:10.1029/2012GL052638.

Briefly about the derecho event over Poland in 11 August 2017

JAN PARFINIEWICZ¹, PIOTR BARAŃSKI², WOJCIECH GAJDA¹, JERZY KONARSKI³, WITOLD INTEREWICZ¹,
WIESŁAW LAZAREWICZ¹, JAN WALASEK¹

¹ *Institute of Meteorology and Water Management - National Research Institute, Warsaw, Poland*

² *Institute of Geophysics, Polish Academy of Sciences, Warsaw, Poland*

³ *CloudFerro sp. z o.o. (CF)*

1 Introduction

The derecho of 11 August 2017, commonly known as Suszek, was the most catastrophic weather event in Poland of the last decade. This case of a violently and very fast moving MCS is very different from the cases of tornadoes generated by the classical, large and slowly moving supercells (Parfiniewicz and Baranski, 2014). Here, the jet stream, located, above the western border of Poland, decided about supporting convection and moving it to the northeast (Taszarek et al., 1919). To divide the day of the considered violent derecho incident into the particular stages of its evolution, we used 144 scans of the Virtual Fujita Scale [VFS] obtained from the PERUN (here PERUN is the own name of Polish lightning location and detection network operated by the IMWM-NRI) lightning data and according to the formulas described previously in the COSMO Newsletters No. 13, 14, 16. It resulted that this particular day with derecho incident was divided into 3 different stages of its development, i.e., the 1-st stage occurring before 04:40 UTC and obeying the very strong storm convection preceding the derecho episode, the 2-nd lasted from 04:50 to 12:30 UTC as the intermediate stage and finally the 3-rd one lasted from 12:40 to 23:50 UTC as such catastrophic episode of violent convection which swept over Poland. Let us note, after (Mańczak et al., 2021), that the detailed synoptic analysis confirmed that the 1-st stage was especially "important for the development of the synoptic situation". It was also confirmed by reports from the European Severe Database (see also Lelatko I., 2020) that were given in the time interval from 10.08.2017 09:00: UTC to 11.08.2017 03:00 UTC. In turn, the time moment 12:40 UTC was accepted as the beginning of the 3-rd stage. Then the linear storm zone from the South Bohemia changed the direction of movement from the SEE-NNW to SSW-NNE. In practice, this direction remained unchanged until the end of the derecho episode, i.e. until 23:50 UTC.

Key words: Derecho, convection, convection system, propagation path, movable filter, lightning location system. **Brief characteristics of the 3 stages**

2 Propagation of the convection system in the 3rd stage.

The reconstruction of the disturbance propagation can be estimated from the wind trajectories, the path of destruction, and direct tracing of the movement of storm cells. In our study of this episode we have used the procedure of sliding movable filters on sixty-eight 10-minute scans from the PERUN lightning location and detection system storm telemetry, that turned out to be effective and relevant. The essence of the approach is the coherence of the images of electrical activity manifested in the neighboring scans (we assume that the 10-minute resolution allows the recognition of basic identities).

The first attempt was to identify propagation leaders. It turned out that while storm cells (clustered together) allow them to be unequivocally identified, the designation of "propagation leaders" is not distinctly expressed because the cells exchange "leadership". This is how the first version of the main and side track was created. Then, using the moving filter method, the weighted average on the filter and the variant division into left and

right paths were determined. The detailed analysis of individual scans shows that around 19:30 the process of propagation splitting into 2 paths begins. At 21:30 the convection system is definitely divided into two branches - one blow (the right track end) went to Kurland and the other to the Bay of Gdańsk. The final dissipation of this stage, as based on the EA evaluation, begins and lasts until 23:50.

The above estimated propagation paths were used to determine the speed of disturbance displacement. The total distance - 864.42 km, traveled in 11.17 hours. with an average speed of 21.50 m/s (77.4 km / h). The highest speeds (up to 40 m/s) were estimated during the propagation splitting stage (from 19:30 to 21:30 UTC) and separating the track into two branches left and right. The right branch remains the main branch and the speeds have been estimated on it. The estimated speed is derived from the position which was determined by the moving filter. We have illustrated such assessment by the example given below for two neighboring scans, i.e., for the time 21:20 and 21:30.

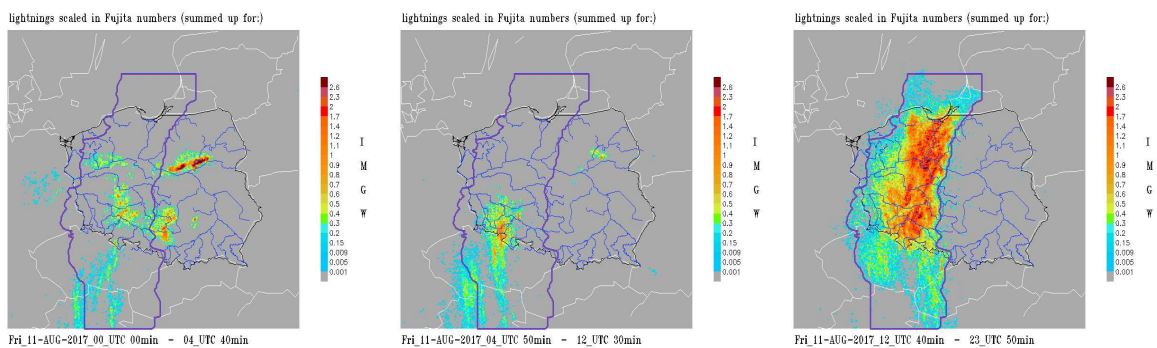


Figure 1: Fig.1. Electric Activity (EA) summary maps (signatures) of the „F (x, y, t) =∫ Fmax (x, y) /time type in Fujita numbers (VFS). The 3rd stage explains and defines the event ”mask” as the boundary of the area of all detected lightning discharges in this stage.

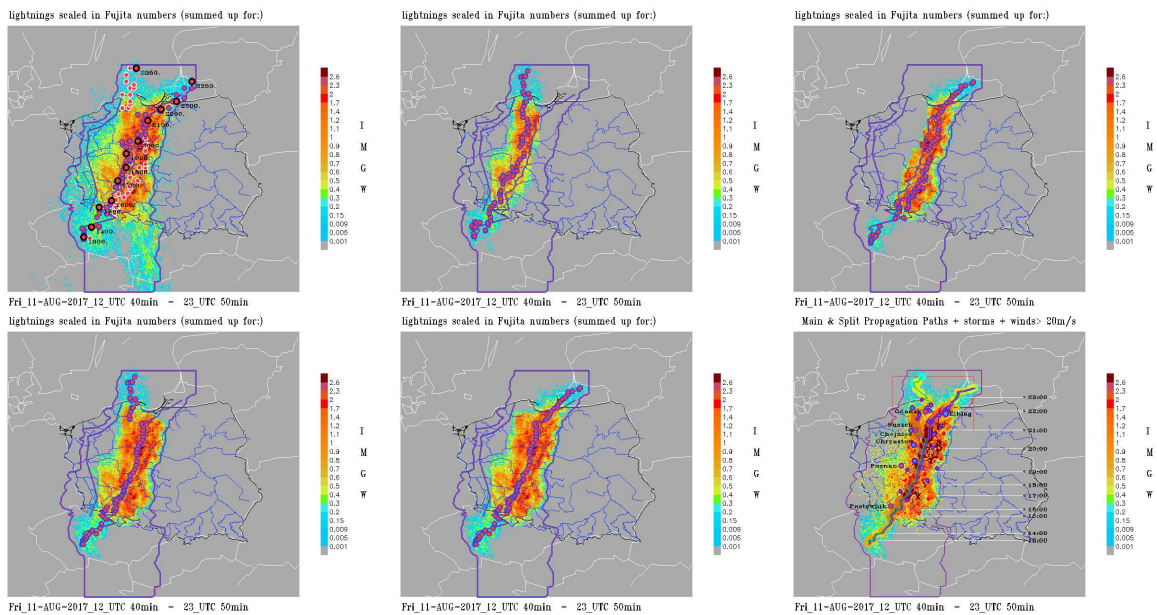


Figure 2: [2.1-2.6]. Estimation of the disturbance propagation path. Subsequent estimates: Fig.2 / [2.1] main and side track, Fig.2 / [2.2-2.3] separated left and right tracks, Fig.2 / [2.4-2.5] left and right tracks on the entire filter, Fig. 2 / [2.6] final (merged) result including the process of propagation splitting.

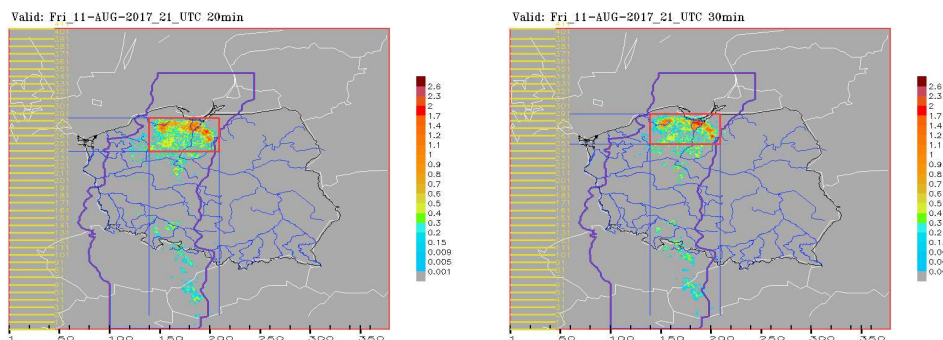


Figure 3: [3.1-3.2] "Movable filter" - a tool that allows to define the current position of the active disturbance area in relation to the calculation grid used (here COSMO 2.8km). The example concerns 2 neighboring scans 21: 20,21: 30.

On the basis of the main path, it was possible to estimate the propagation velocities.

3 Supplements

3.1 Example of reflectivity scans for Gdańsk and Poznań

To understand the considered strong convection process it requires a separate detailed non-hydrostatic diagnosis (≈ 0.3 km) with assimilation procedure that includes Doppler winds on each of the 68 scans. Conducting of such task takes a lot of time and work. So far, quasi 3D reflectivity scans for Poznań and Gdańsk have been made. Below we present them for two selected time moment: for 17:00 UTC given by the reflectivity in dBZ together with the Doppler wind for the alleged formation of supercell and for 21:30 UTC, , i.e., obtained after 50 min. from the estimated moment of split.

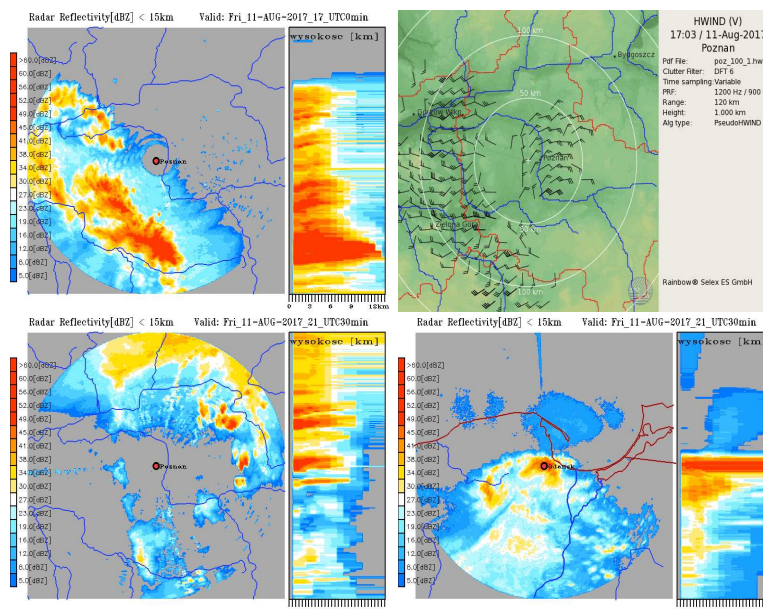


Figure 4: [4.1-4.4]. Doppler & Quasi 3D scans (maxcappi Z - XY, and X - ZY) of reflectivity for Poznań and Gdańsk. The scans were preceded by interpolation of the measured reflectivity (Z: 1km -18km, XY: 0.7 km) to the computational grid with dz = 250m.

At this time the signature of bow echo and rear inflow jet are rather weak to see. But what is characteristic in this case, is the vertical cylinder of maximum reflectivity that is reaching the stratosphere. Here, it should be noted for clarification, that after 20 minutes later, both bow echo and rear inflow jet are emphatically expressed.

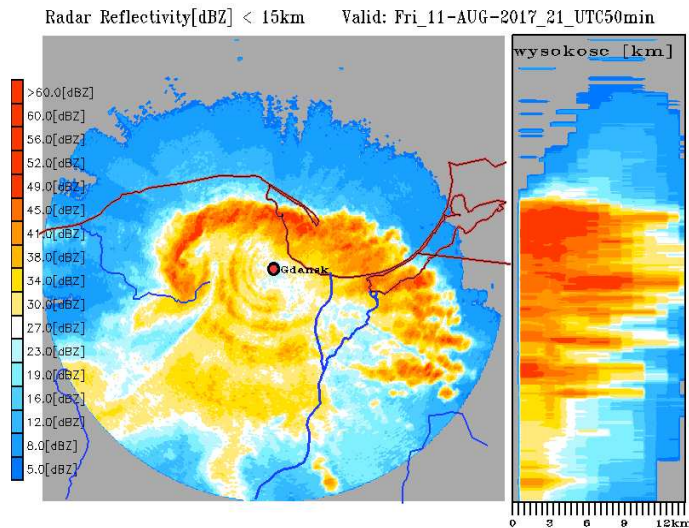


Figure 5: Quasi 3D reflectivity scan for Gdańsk radar at 21:50 UTC showing a clear bow echo and rear inflow jet/RIJ structure.

3.2 Looking for the coherent impact structures connected to the considered derecho incident.

Two results obtained from the simulation with the COSMO 2.8 km model with a time resolution of 15 minutes are worth presenting.

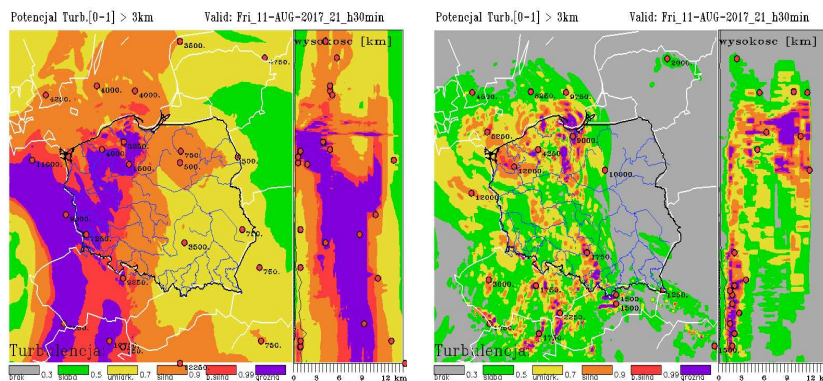


Figure 6: [6.1-6.2]. Slightly modified results of operational forecasts of turbulence over Poland broken down into 2 components of Reynolds and Richardson in the “maxcappi” Z-XY and X-ZY system; Z axis: 0-15 km.

These calculations are derived from an operational turbulence forecasting tool. Here they have been divided into 2 components, i.e. Reynolds and Richardson numbers, respectively. The Reynolds number, let’s recall it here $\alpha^* \rho^* V$ is just momentum. Another association is root square of kinetic energy. The Richardson number, as is well known, is measure of atmosphere stability. Generalizing the Bernoulli principle, these quantities - especially energy and momentum - should be invariants of the trajectory. Thus, the momentum in particular,

indicates well that the sources of ground wind force are related to the middle and upper troposphere. Here, it should be noted that also the GFS analysis for the level of 300 mb has located jet stream over the western border of Poland.

3.3 Wind through trajectories

For several years, the operational weather service has been calculating the 850 mb trajectories for selected four stations in Poland. The ones presented below well reflect the wind dynamics during the considered derecho day.

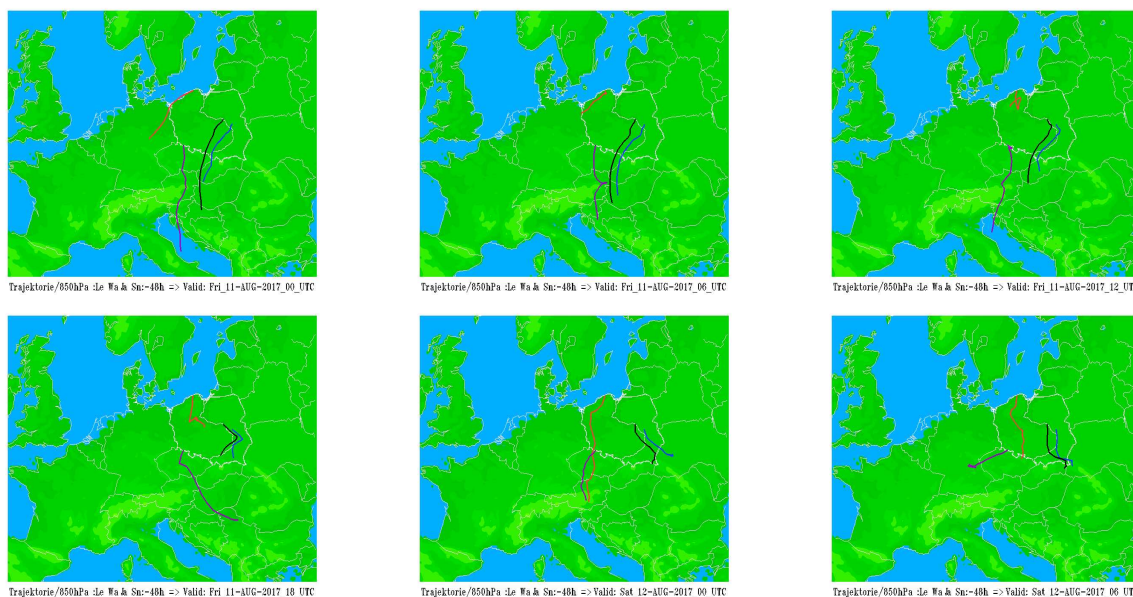


Figure 7: [7.1-7.6]. Trajectories for the level of 850 mb and the time interval of 48 hours and for 4 selected places in Poland, i. e., for Leba, Jarczew, Śnieżka and Warsaw from the dates: 2017081100, 2017081106, 2017081112, 2017081118, 2017081200 and 2017081206.

4 Conclusions

In light of electrical activity it was not a strong convective event (max 3.6 VFS). This indicates that the decisive factor here was the forcing of the synoptic scale, possibly related to the middle and upper troposphere, and even the stratosphere (case 17:00 over Poznań, case 21:30 over Gdańsk). The highest estimated speeds (up to 40 m/s) occurred around 19:30 UTC, preceding the split stage. The estimated velocity of propagation compared with the telemetry data and damage measurements, especially in the stage from 19:30 to 21:30 UTC, have matched the VFS numbers quite well. Understanding the process requires a separate detailed non-hydrostatic diagnosis (Δz 0.3 km) with assimilation procedure that includes Doppler winds on each of the 68 scans, and then merging these 68 domains (3D fields of meteorological elements) into one whole. This is just an introduction and an incentive to achieve this goal. As for the forecast, the collected material allows any thunderstorm prediction method to be validated. The results of the operational calculations using the stability indices method (LPP: Lityńska, Parfiniewicz, Piwkowski 1976) and the "thunderstorm thermometer" approach (Parfiniewicz 2014) are promising (Barański and Parfiniewicz 2019).

References

- [1] Litynska Z., Parfiniewicz J. and H. Piwkowski, "*The Prediction of Airmass Thunderstorms and Hails*," W.M.O. Bull, Vol. 450, 1976, pp. **128-130**.
- [2] Aligo, E. A., Gallus, W. A. and Segal, M., 2007: Summer Rainfall Forecast Spread in an Ensemble Initialized with Different Soil Moisture Analyses. *Wea. Forecasting*, 22, **299-314**.

Summary of Results from the COSMO Priority Project CARMA: Common Area with Rfdbk/MEC Application

A. IRIZA-BURCA¹, F. GOFA², D. BOUCOUVALA², T. ANDREADIS², J. LINKOWSKA³, P. KHAIN⁴, A. SHTIVELMAN⁴, F. BATIGNANI⁵, A. PAULING⁶, A. KIRSANOV⁷, T. GASTALDO⁸, B. MACO¹, M. BOGDAN¹
AND F. FUNDEL⁹

¹NMA, ²HNMS, ³IMGW-PIB, ⁴IMS, ⁵COMET, ⁶MCH, ⁷RHM, ⁸Arpae-SIMC, ⁹DWD

1 Introduction and Short Overview of the MEC-Rfdbk System

Before the start of PP CARMA (Common Area with Rfdbk/MEC Application), Common Plot (CP) verification Activities were carried out using the VERSUS verification software environment. In recent years, partly due to technical limitations of VERSUS and lack of further development, the possibility of utilizing multiple verification modules that would not necessarily be linked to one software package was considered (e.g. VAST software for spatial methods). However, it is essential to maintain a common tool for the CP Activities, in order to ensure the adoption of the same verification practices and allow the long-term monitoring of the derived results (Gofa et. al, 2015; Gofa, 2016).

The MEC-Rfdbk system replaced the VERSUS software environment as a Common Verification Software (CVS), in order to perform part of the verification activities in the consortium. The main use of the new CVS is the production of the CP verification, with spatial verification performed with other available COSMO tools (VAST, etc.). A centralized transfer and visualization of CP statistics on COSMO web server also facilitates the easier analysis of the outcome of CP activities and was also one of the main deliverables of the project. Although MEC-Rfdbk is also suitable for EPS verification, this type of application was not included in the CARMA project, due to the fact that EPS verification is not part of CP activity.

The Model Equivalent Calculator (MEC; Potthast, 2016) software for the production of Feedback Files (FF) (<http://cosmo-model.org/content/model/documentation/core/\\cosmoFeedbackFileDefinition.pdf>), and verification scripts based on the R libraries Rfdbk (Fundel, 2021), are tools that were developed and are in operational use at DWD for the verification of both COSMO and ICON model chains. The three main components of the MEC-Rfdbk verification system (figure 1) are:

- MEC: used to produce FF based on model output and observations in netcdf format; results stored also in NetCDF format (FF);
- Rfdbk: used to compute statistical scores using the FF produced by MEC; results stored in Rdata format;
- Shiny web-server: used to visualize the results (COSMO web server).

The FF are produced by the Model Equivalent Calculator (MEC; Potthast, 2019) within the data assimilation system or as stand-alone. For the purpose of this project and the first test of the system, FF were produced using a common set of observations retrieved in bufr format from the ECMWF MARS archive. These observations were converted to NetCDF format with the bufr2netcdf software (Patrino and Cesari, 2011) and used as input in MEC. Further on, these feedback-files are used by the Rfdbk (Fundel, 2021) package to calculate the verification scores. Finally, the verification scores in Rdata format are visualized on the dedicated COSMO web page, using the R Shiny Server (Wang et al., 2020). This centralized, online and interactive visualization of the results on the COSMO web-site using the R Shiny Server is meant to enable a easy and interactive evaluation of the results.

doi:10.5676/dwd_pub/nwv/cosmo-nl_21_04

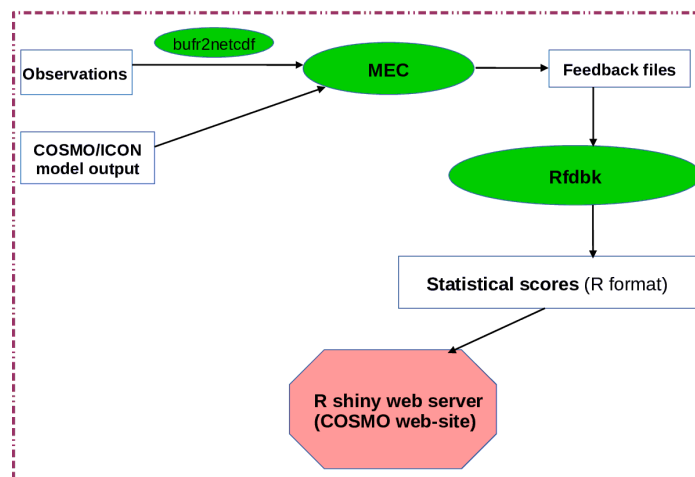


Figure 1: Schematic representation of the MEC-Rfdbk system.

2 Overview of System Implementation

The main outcome of the project was the implementation of the new CVS in most COSMO countries, with the system already in use for various operational implementations of both COSMO and ICON (depending on model data availability), as can be seen from tables 1 and 2.

	IMPLEMENTATION		PRODUCTION		Visualization (optional)
	DACE/MEC	Rfdbk	FF	SCORES	
NMA	yes	yes	yes	yes	yes
HNMS	yes	yes	yes	yes	-
DWD	*yes	*yes	*yes	*yes	*yes
MCH	*yes	*yes	on going	on going	
CoMET	yes	yes	yes	yes	
IMGW	yes	yes	yes	yes	yes
RHM	yes	yes	on going		
IMS	yes	yes	yes	yes	yes
ArpaE	yes	on going	yes	on going	

Table 1: Status of implementations for the MEC-Rfdbk system in each center.

* denotes that the system was installed and in use before the start of the project.

	NMA	HNMS	DWD	MCH	CoMET	IMGW	RHM	IMS	ArpaE
COSMO	x	-	x	x	x	x	-	-	x
ICON	x	x	x	x	-	-	x	x	-

Table 2: Overview of models verified by each center using the MEC-Rfdbk software.

First applications based on MEC-Rfdbk for CP activities started in the 2020 spring season (MAM 2020), while the number of model scores computed with the new CVS has gradually increased until present (14 models expected for JJA2021). Following the finalization of the project, a few remaining issues are at the moment still on-going, due to some limitations either of the software or specific problems of some users (e.g production of FF from the IFS model). These activities are included in the COSMO-SPRT (Support) Common Plot activities for 2021-2022. As Common Plot activities are a continuous and evolving task, some features of the current requirements might differ to the ones envisioned at the beginning of the project. As a consequence, follow up activities will also aim to incorporate the new requirements included in this year guidelines of the CP activity (e.g. upper air verification, 6h precipitation in all time intervals, conditional verification and update of the system with new versions of the software).

For detailed description of the MEC-Rfdbk system and results obtained during the project, we refer to the documentation presented in Section 4.

3 Timeline of Results

For the various results obtained during the CARMA project and exemplified in the sections below, the following models were employed:

- ICON GLOBAL, ICON-EU, ICON-D2, COSMO-D2 (DWD)
- COSMOPL7 / COSMO-PL, ICONPL, COSMO-CE-PL, COSMOP2k8 (IMGW-PIB)
- COSMO_ME, ICON_IT2, COSMO_IT2 (COMET)
- ICONGR (HNMS)
- ICON_IMS / ICON_IL2p5 (IMS)
- COSMO-1E, COSMO-2E (MCH)
- COSMO-RO_2p8, ICON-RO_2p8, COSMO-RO (NMA)

Standard Verification (seasonal) is generally performed for the following continuous parameters: 2-meter temperature - T2M (deg K), 2-meter dew point temperature - TD2M (deg K), surface pressure - PS (Pa), total cloud cover - N (octa), 10 meter wind speed - FF (m/s), wind direction - DD (deg) and wind gust - Gust (1 hour, m/s). Categorical scores are also computed, for the following parameters: 6 hour accumulated precipitation - RR_6h (thresholds: 0.2, 1, 5, 10, 15, 20 mm/6h), total cloud cover (*thresholds* ≥ 1 , ≥ 4 and ≥ 7) and 10-meter wind gust (*thresholds* ≥ 12.5 , ≥ 15 , ≥ 20 m/s).

Scores for continuous parameters include the mean error (ME) and root mean squared error (RMSE), mean absolute error (MAE), standard deviation (SD) and the correlation coefficient (R2) (only ME and RMSE will be discussed in the following examples). Dichotomic scores include the probability of detection (POD), false alarm rate (FAR), equitable threat score (ETS) and frequency bias (FBI). Other scores based on the number of hits, misses, false alarms and correct negatives respectively are also available. For all scores, the number of observations used in computations (LEN) is also available as well as the observation mean (OMEAN) and the forecast mean (OMEAN).

For the purpose of the project and future Common Plot Activities, scores are computed either for national domains or for the two domains used in the Common Area Verification Activities (see figure 2).

The two areas were initially defined according to the list of stations previously used in verification activities with VERSUS. The results are computed taking into account all stations of interest. However, results are also available stratified by station altitude. Starting with the JJA2021 season, common area stratification is defined by polygons instead of station lists.

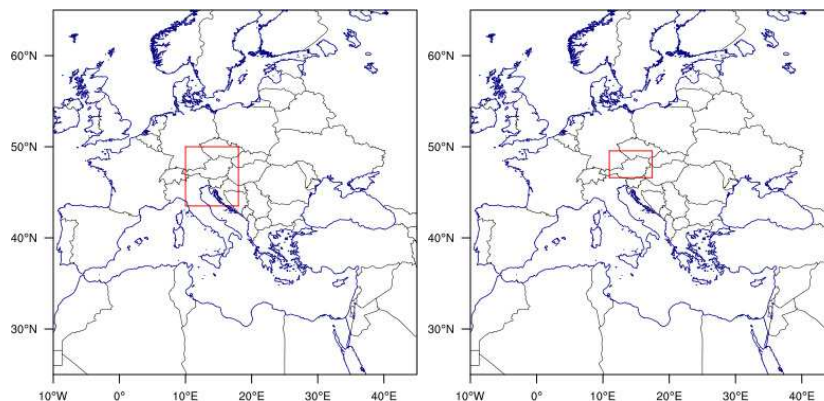


Figure 2: Common Areas: CA1 (left) and CA2 (right) used for the verification.

The verification results exemplified in the following sections are a sample of the derived statistics that were gradually obtained following the implementation of the MEC-Rfdbk system in more participating institutes. Complete sets of statistical scores obtained with the MEC-Rfdbk verification system for the models considered for the project are either available on the COSMO shiny server (<http://www.cosmo-model.org/shiny/apps/carma/>) or detailed in various papers referenced hereafter, including the Common plot annual reports available on the COSMO web site (<http://cosmo-model.org/content/tasks/verification.priv/default.htm>).

For a detailed description of the Common Area Verification Activities, we refer to the document by Gofa et al (2021).

The first results of a cross model verification (with the MEC-Rfdbk software) for the Common Plot activities were performed for the 2020 spring season (**MAM 2020**) and are detailed in Iriza-Burca, Linkowska and Fundel (2020). For these results, a set of three COSMO model runs were considered: COSMO-D2 (DWD), COSMO-PL (IMGW) and COSMO-RO (NMA). Only COSMO 00 UTC model runs were evaluated, with forecast step every 3 hours. The integration domains for COSMO-D2 and COSMO-PL were the operational ones (also included in the official Common Plots activities), while the COSMO-RO integration domain differed from the operational set-up of the model employed in NMA (in order to cover the Common Areas). The scores were computed for the two common areas of interest for Common Plot Activities.

Following the first seasonal verification results obtained for MAM2020, some verification results using the MEC-Rfdbk system were included in the ICON Report “Verification of ICON in Limited Area Mode at COSMO National Meteorological Services” (Rieger et. al, 2021) published as part of the Priority Project “Transition of COSMO to ICON” (PP C2I). This report offered the first published verification results regarding the transition for the COSMO national meteorological services to the ICON model.

For this report, verification results for the SON2020 season were obtained either entirely using the MEC-Rfdbk system (e.g. COSMO-RO_{2p8} vs. ICON-RO_{2p8}) or originally with the VERSUS verification software and then translated to Rdata in order to visualize them using Rfdbk/Shiny server (COSMO-CE-PL vs. ICON-PL and Common Area Verification Results).

Starting with the 2021 winter season (**DJF2021**), the first complete results obtained with MEC-Rfdbk, were included in the Seasonal Common Verification Results. For the DJF2021 season, FF were produced for 3 models on CA1 (ICON-EU, COSMOPL7, COSMO_ME; figure 3) and 8 models on CA2 (ICON-D2, ICON_IL2p5, ICONGR, ICONPL, COSMO-1E, COSMO-2E, COSMO-D2, COSMOP2k8).

Scores for national domains were also computed for some of the models. Additionally, results from ICON-RO_2p8 and COSMO-RO_2p8 were provided for the corresponding national domain. Due to differences in availability of model data, some model verification results were either computed separately for each model and merged using R scripts developed by HNMS or computed with the VERSUS verification software and translated to Rdata in order to be visualized along with the rest of the models.

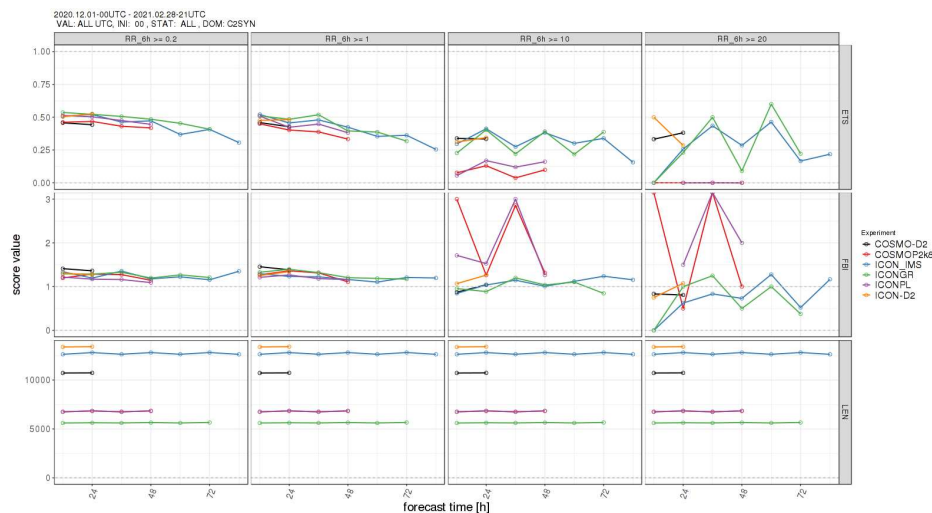


Figure 3: DJF2021 - Categorical scores for RR_6h (CA2): ETS (top), FBI (middle) and number of observations (bottom) values for CA2; thresholds (left to right): $\geq 0.2mm/6h$, $\geq 1mm/6h$, $\geq 10mm/6h$ and $\geq 20mm/6h$. COSMO-D2 (black), COSMOPk28 (red), ICON_IMS/ICON_IL2p5 (blue), ICONGR (green), ICONPL (purple) and ICON-D2 (orange)

The number of models included in the verification activities increased for the **MAM2021** season. For this period, FF were produced from 4 models for CA1 (ICON-GLOBAL, ICON-EU, COSMO_ME, COSMOPL7) and 9 models for CA2 (ICON-D2, ICON_IL2p5, ICONPL, ICONGR, ICON_IT2, COSMO-CE-PL, COSMO-1E, COSMO-2E, COSMO_IT2), again with additional results for national domains (including ICON-RO_2p8, COSMO-RO_2p8).

As can be seen by the number of observations used for the computation of statistical scores for continuous variables (figure 4), the differences in availability of model data was reduced compared to the previous season, with results from more models computed simultaneously and directly with MEC-Rfdbk, instead of being computed with the VERSUS verification software and translated to Rdata for visualization.

Compared to the previous seasons, starting with **JJA2021**, a polygon description will be employed for the verification area instead of the previously used station lists. Also starting with the JJA2021 season, TEMP verification scores obtained with the MEC-Rfdbk verification system will be gradually included in the Common Plot activities.

For the JJA2021 season, FF are expected to be produced from 4 models for CA1 (ICON-GLOBAL, ICON-EU, COSMO_ME, COSMOPL7) and 9 models for CA2 (ICON-D2, ICONGR, ICON_IL2p5, ICON_IT2, ICONPL, COSMO_IT2, COSMO-CE-PL, COSMO-1E, COSMO-2E). For national domain verification, 12 models are expected to be included (from CA1 and CA2, additionally ICON-RO_2p8, COSMO-RO_2p8). Also starting with this season, upper air verification based on TEMP observations will be included in the Common Plot Activities, after tests for individual domains/models during PP CARMA.

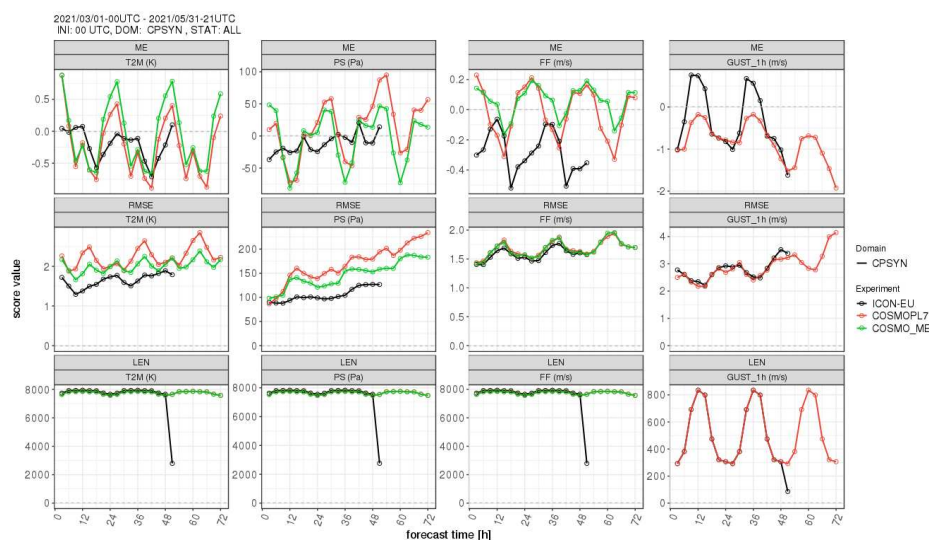


Figure 4: MAM2021 - ME (top), RMSE (middle) and number of observations (bottom) values for CA1; left to right: T2M, PS, FF and GUST (1h). ICON-EU (black), COSMO-PL7 (red) and COSMO_ME (green)

4 Conclusions and Available Documentation

Following the finalization of the CARMA project, it can be concluded that the MEC-Rfdbk system is implemented and runs operationally in IMGW-PIB, IMS, NMA, HNMS and COMET for various configurations of the ICON and COSMO models. As previously mentioned, the system was already in use before the start of the project in MCH (surface verification only) and DWD. The following type of graphs are produced with the MEC-Rfdbk system for Common Plot Activities:

- Categorical scores for Gust, RR_6h and N;
- Scores for continuous parameters;
- Scores for upper air parameters;
- Comparison between two models showing the trend in different scores.

All the remaining open issues that concern MEC-Rfdbk adaptation in some services and implementation of new features, will be performed through WG5 SPRT Common Plot activity. Detailed documentation and templates for the use of the MEC-Rfdbk system are available for usage both for CP and national verification activities. For more detailed presentations of the MEC-Rfdbk system and its components, including information regarding installation and use, documentation is available in the COSMO repository (PP CARMA Branch): <http://cosmo-model.org/view/repository/wg5/PP-CARMA>.

How to install

http://cosmo-model.org/repository/wg5/PP-CARMA/Task1/Install_notes_CARMA_v1.5.pdf

How to use

(example based on NWP Test Suite @ECMWF;
COSMO Repository) NWPTest-Suite_Doc4CARMA.docx

About Rfdbk

Ffverificationsuite@DWD.docx (also on COSMO Repository) <http://www.cosmo-model.org/shiny/users/fdbk/RfdbkVeriDoku.html>

About feedback files

Ffverificationsuite@DWD.docx (also on COSMO Repository) <http://www.cosmo-model.org/shiny/users/fdbk/RfdbkVeriDoku.html>

General Guidelines (COSMO repository)

http://cosmo-model.org/repository/wg5/PP-CARMA/Task1/CARMA_guidelines.pdf

References

- [1] A. Iriza-BURCĂ, J. Linkowska, F. Fundel (2020): Common Area Verification Activity with Rfdbk/MEC Application: MAM 2020 First Results. COSMO Newsletter, No.20 (p.18-30), DOI: doi:10.5676/dwd_pub/nwv/cosmo-nl_20_04
- [2] Feedback-File definition (2012): Supplementary Documentation, DWD, <http://cosmo-model.org/content/model/documentation/core/cosmoFeedbackFileDefinition.pdf>
- [3] F.Fundel (2021): Feedback File Verification Suite at DWD, DWD, available online at <http://www.cosmo-model.org/shiny/users/fdbk/RfdbkVeriDoku.html>
- [4] F.Gofa (2021): Common Verification Plots Guidelines for 2021-22 (www.cosmo-model.org/content/tasks/verification.priv/common/reports/CP-2021-2022.pdf),
- [5] F. Gofa (2016): COSMO Verification Overview, 38th EWGLAM and 23th SRNWP Meeting, Rome, 03-06 October 2016
- [6] F. Gofa, U. Pflüger, X. Lapillonne, A. Vocino, D. Boucouvala, J. Linkowska, R. Dumitrache, A. Bundel, M.S. Tesini, E. Oberto, Y. Levi (2015): Recommendations: Strategy on Verification Tools
- [7] P. Patrino, D. Cesari (2011): Wreport-bufr2netcdf: a free library and tools for decoding BUFR reports and creating input files for COSMO-Model assimilation, 13th COSMO General Meeting, 5-9 September 2011, Rome (Italy), Parallel session: WG1 and PP KENDA. Available on-line at: <http://cosmo-model.org/content/consortium/generalMeetings/general2011/wg1.htm>.
- [8] R. Potthast (2019): Model Equivalent Calculator (MEC) overview, 21st COSMO General Meeting, 9-13 September 2019, Rome (Italy). Available on-line at: <http://cosmo-model.org/content/consortium/generalMeetings/general2019/default.htm>
- [9] D. Rieger, M. Milelli, D. Boucouvala, F. Gofa, A. Iriza-Burca, P. Khain, A. Kirsanov, J. Linkowska, F. Marcucci and the C2I team (2021): Verification of ICON in Limited Area Mode at COSMO National Meteorological Services. Reports on ICON, Issue 006, ISSN: 2628-4898, DOI: https://doi.org/10.5676/dwd_pub/nwv/icon_006, June 2021
- [10] W. Chang, J. Cheng, J.J. Allaire, Y. Xie, J. McPherson (2020): shiny: Web Application Framework for R. R package version 1.5.0. Available online at: <https://CRAN.R-project.org/package=shiny>

Common Area Results 2020-2021

COSMO WG5: VERIFICATION AND CASE STUDIES

Flora Gofa (fgofa@hnms.gr)

Abstract

Verification results of statistical indices for main weather parameters are derived using the operational COSMO and ICON-LAM model implementations in each service. The domain (common), the resolution, the statistical scores/methods and the graphical representation approaches, are decided on an annual basis from WG5. A common verification software is used in most cases which allows for a homogeneous, standardized and objective way to apply, calculate and present the verification scores. The outcome of this activity provides a basis to monitor the performance of the models model and track the systematic errors. Since the introduction of ICON-LAM in the operational forecast procedure of some services, special focus is given to the relative performance of the two models. In this report, statistical results of JJA-2020 up to MAM 2021 model performance are presented.

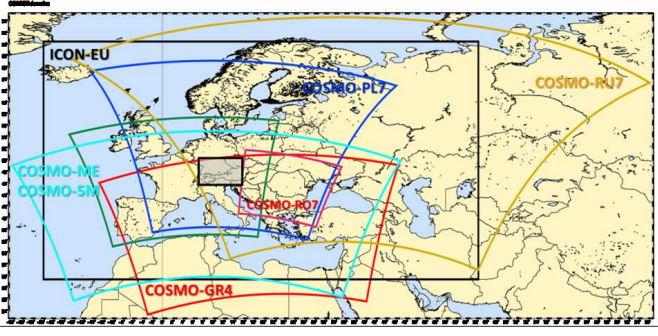
Keywords: Verification. Common Plots, FSS

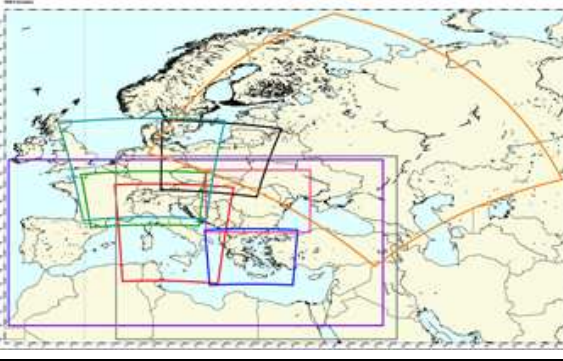
1 Overview

COSMO has implemented a procedure to perform homogeneous and comparable evaluation of model performance, which includes the calculation of verification scores over a common area, with the same observations, same methods and when possible with the same verification software. Verification results of statistical indices for main weather parameters derived using the operational COSMO and ICON-LAM model implementations in each service. The domain (common or custom), resolution, statistical scores/methods, frequency and graphical representation, are decided on an annual basis from WG5. The main findings of this organized analysis is presented during the GM plenary session together with the long term trend of them, providing a basis to track the performance of model. The use of common verification software allows for a standardized and objective way to apply, calculate and present the verification scores. Preparation of observation data and calculation of seasonal statistics are based on the guidelines that are derived on an annual basis from WG5. ICON-LAM models statistical results are included from any of the various services that use the model operationally. For JJA2020 and SON2020 analysis, only few centres have distributed ICON-LAM forecasts for evaluation but in the following seasons, COSMO has been gradually substituted with ICON-LAM especially for fine resolution implementations. Selective verification results of COSMO and ICON-LAM models over Common Area 1 (ComA1) and Area 2 (ComA2) are presented below while the complete selection of statistical results can be found in <https://www.cosmo-model.org/content/tasks/verification.priv/default.htm>.

2 Areas of Verification

The areas and specifications for model performance evaluation are presented below. In ComA-1, models with coarser resolution are included, while the higher resolution COSMO and ICON-LAM models are compared over ComA-2 (Table below).

ComA-1 Area/Specs	
	<p>00UTC Forecast runs Forecast Horizon: 72h Seasonal: JJA20, SON20, DJF21, MAM21</p>
Models	<p>Global ICON global, IFS LAMS DWD: ICON-EU COMET: COSMO-ME HNMS: COSMO-GR4 ARPA-E: COSMO-5M IMGW-PIB: COSMO-PL7 RHM: COSMO-RU7, ICON-RU7</p>

ComA-2 Area/Specs	
	<p>W10.963, S46.597, E17.437, N49.550 00UTC Forecast run Forecast Horizon: 48h Seasonal: JJA20, SON20, DJF21, MAM21</p>
Models	<p>LAMS DWD: COSMO-D2, ICON-D2 COMET: COSMO-IT, ICON-IT HNMS: ICON-GR2.5 ARPA-E: COSMO-2I IMGW-PIB: COSMO-PL2.8, ICON-PL2.5 MCH: COSMO-1E, COSMO-2E IMS: ICON-IMS</p>

3 Results

3.1 Common Area 1

The models are evaluated in terms of Mean Error and Root Mean Square Error indices for the continuous parameters, using SYNOP observations over the Common Area domains using either VERSUS or MEC-Rbdfk software. Summary plots of continuous parameters are shown in plots 1a-d below,

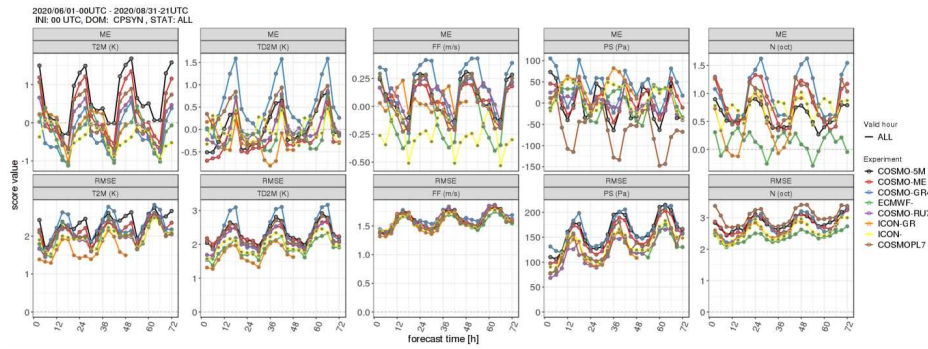


Figure 1: ME (first row) and RMSE (second row) for (from left to right) T2M, TD2M, Wind Speed, Pressure, Total Cloud Cover indices calculated over ComA-1 (JJA2020)

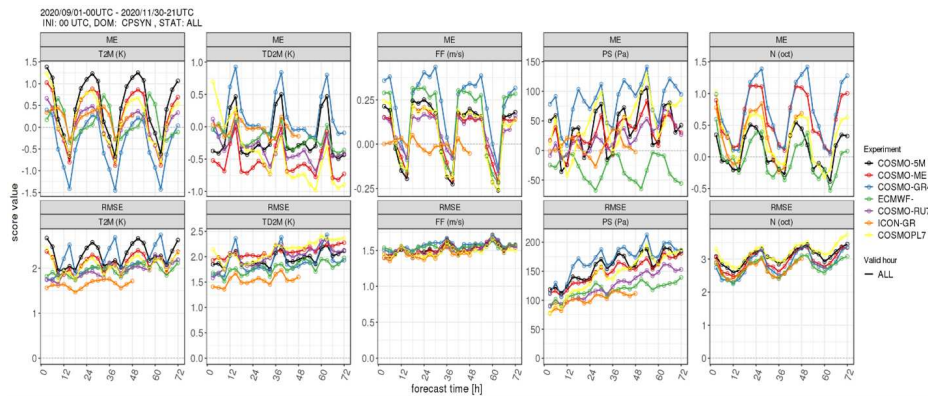


Figure 2: ME (first row) and RMSE (second row) for (from left to right) T2M, TD2M, Wind Speed, PS, Total Cloud Cover indices calculated over ComA-1 (SON2020)

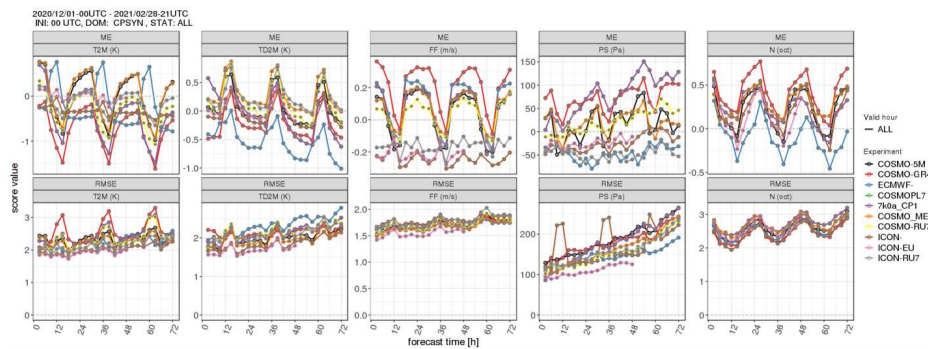


Figure 3: ME (first row) and RMSE (second row) for (from left to right) T2M, TD2M, Wind Speed, PS, Total Cloud Cover indices calculated over ComA-1 (DJF2021)

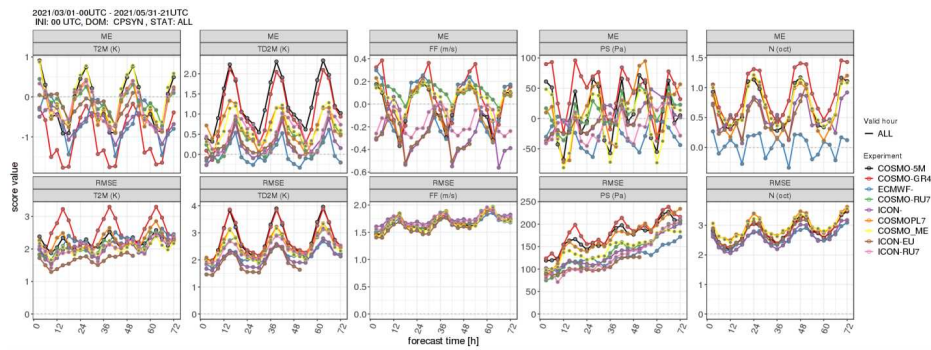


Figure 4: ME (first row) and RMSE (second row) for (from left to right) T2M, TD2M, Wind Speed, PS, Total Cloud Cover indices calculated over ComA-1 (MAM 2021)

For ICON models (ICON, ICON-EU, ICON-RU) and for IFS, the bias diurnal cycle is weaker and RMSE values are reduced for T2m and Td2m. RMSE wind speed is higher in warm hours of the day and comparable for all models in all seasons. The night time WS overestimation however which is a typical systematic error with both COSMO and IFS models for all seasons, is not apparent on ICON-LAM models, which exhibit a much weaker daily cycle, and an almost constant underestimation which is greater in JJA and MAM afternoon hours. RMSE for PS is reduced for ICON models, especially compared to COSMO ones and is similar to IFS forecasts. However, the tendency of PS RMSE increase with forecast time for all seasons and the diurnal cycle for JJA are comparable. PS bias is irregular for all seasons, and a more distinct difference is shown in DJF, with ICON models negative values all over the period, in contrast to positive and slightly time increasing COSMO values. TCC RMSE values and bias diurnal cycles are comparable for COSMO and ICON models with RMSE maximal values at night and better scores for DJF. ICON models produce slightly lower overestimation at night, and only IFS produces a weaker diurnal cycle for all seasons especially MAM. The point-wise 6h accumulated precipitation forecasts are evaluated in terms of categorical indices for different thresholds. JJA2020 and DJF2021 results for ETS, POD and FAR are presented in Figures 2a-b.

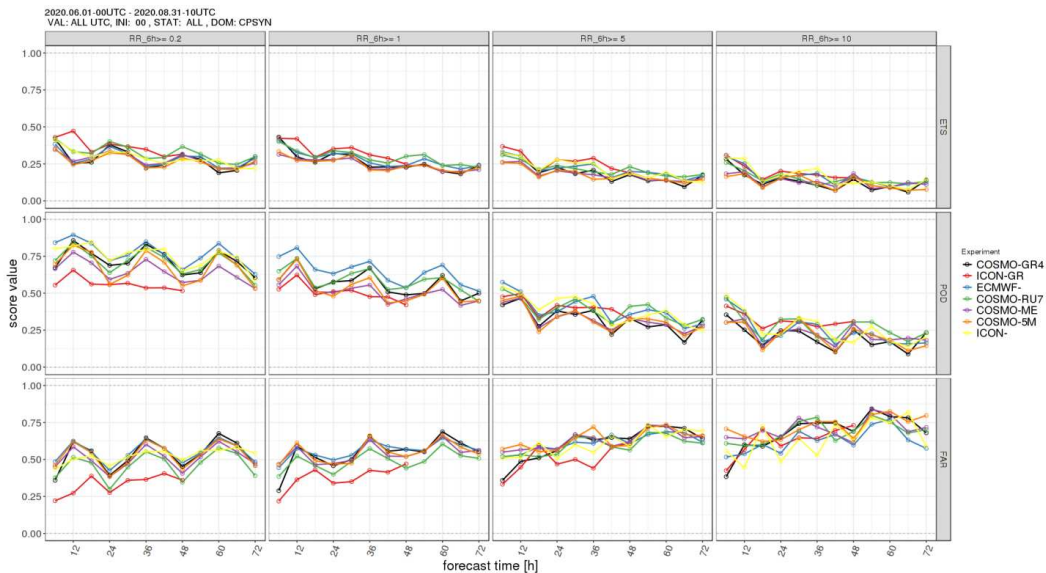


Figure 5: 6h accumulated precipitation indices for different thresholds. From top to bottom (ETS, POD, FAR). From left to right (0.2, 1, 5, 10mm) for JJA2020.

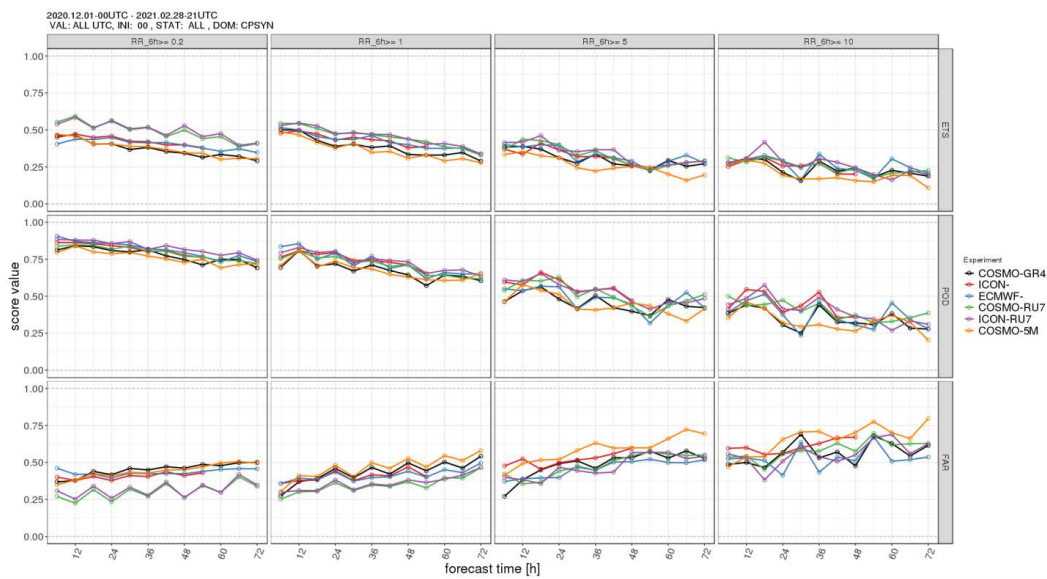


Figure 6: 6h accumulated precipitation indices for different thresholds. From top to bottom (ETS, POD, FAR). From left to right (0.2, 1, 5, 10mm) for DJF2021.

As in previous years, the diurnal cycle of the scores is distinct for JJA season and score trend worsens with forecast time and increasing threshold. Differences among ICON and COSMO models are not so distinct. However, for small precipitation thresholds, there is a slight improvement in ETS for ICON-GR, a clearer improvement in FAR and slight worsening for some model implementations in POD in JJA. This outcome reveals a dryer behaviour of ICON forecasts for that season compared to the observed values.

The results in the higher thresholds are quite variable and this can be attributed also to the smaller sample size. In DJF, the scores generally improve, they are more consistent while the diurnal variation is weaker. ICON-RU7 and COSMO-RU7 present similar behaviour, with better values of ETS and FAR than other models for low thresholds.

3.2 Common Area 2

For a better comparison among COSMO and ICON-LAM higher resolution models, they are presented grouped together in order to detect general tendencies or differences that can be attributed to the various implementations. DJF and MAM are the seasons with the greatest ICON-LAM forecasts availability. Temperature, wind speed and TCC results for these two seasons are presented below.

For T2m (Figures 3a,b), the most distinct difference, which is also consistent with coarser resolution models, is the reduced diurnal variability in bias values for ICON-LAM models, which is mostly apparent in DJF, with values closer to zero. The RMSE diurnal variation for DJF is comparable for the two sets of models. However, in MAM season RMSE for ICON models is reduced, with minimal diurnal variability.

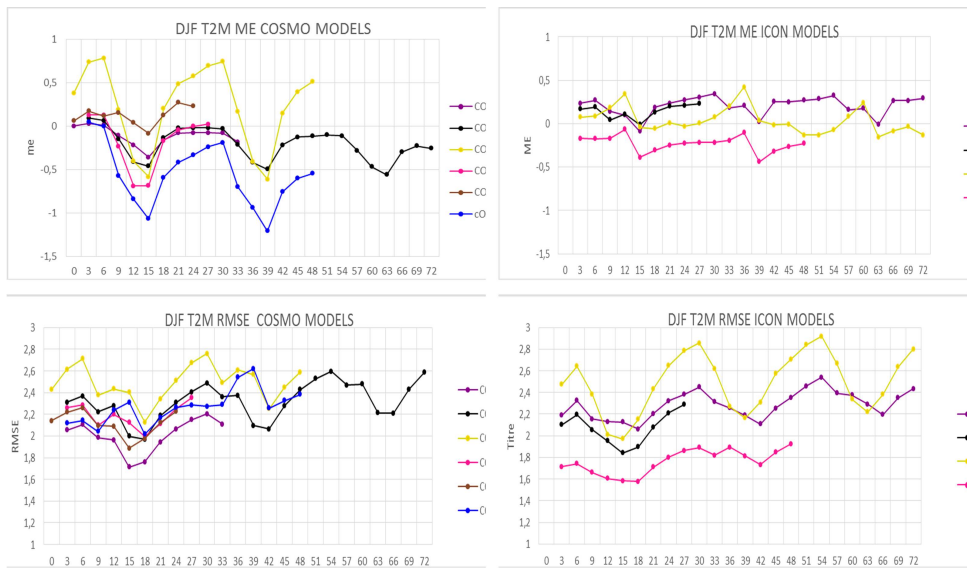


Figure 7: T2m ME (top) and RMSE (bottom). COSMO models (left) and ICON models (right) for DJF2021



Figure 8: T2m ME (top) and RMSE (bottom). COSMO models (left) and ICON models (right) for DJF2021

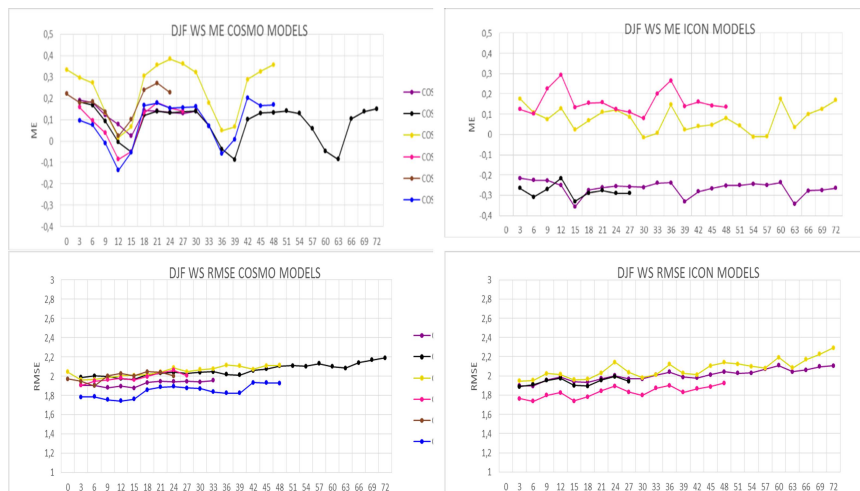


Figure 9: WS ME (top) and RMSE (bottom). COSMO models (left) and ICON models (right) for DJF2021

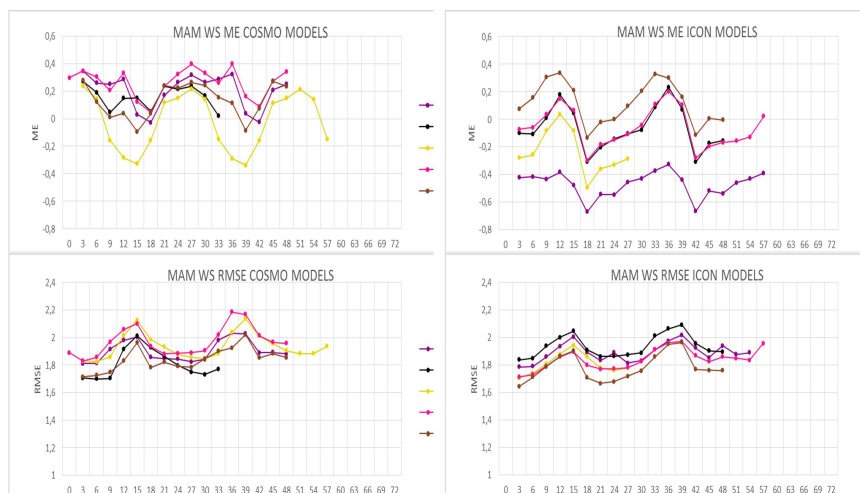


Figure 10: WS ME (top) and RMSE (bottom). COSMO models (left) and ICON models (right) for MAM2021

The indices for wind speed are presented in (Figures 4a,b), The DJF wind speed bias diurnal variation is weaker for ICON models and the negative tendency that was found for coarser resolution is now found in two models, while the RMSE error cycle and range are similar for both seasons, with higher values in warm hours in MAM (Figures 3c,d). Moreover, for MAM, the bias diurnal variability is shifted among the two sets of models, with COSMO overestimation in the early morning hours, while ICON models bias is positive around the afternoon.



Figure 11: TCC ME (top) and RMSE (bottom). COSMO models (left) and ICON models (right) for DJF2021

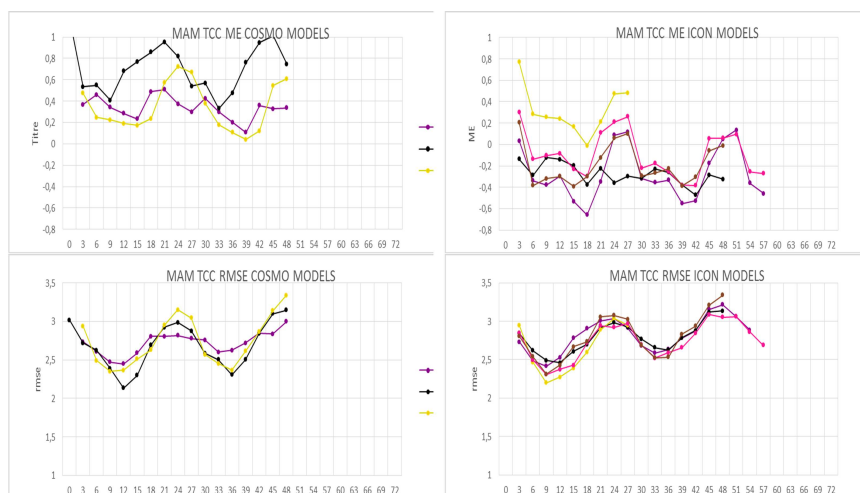


Figure 12: TCC ME (top) and RMSE (bottom). COSMO models (left) and ICON models (right) for MAM2021

The TCC bias difference among the two sets of models is clear, with ICON models exhibiting a diurnal cycle with underestimation especially in the warm hours for both seasons (Figures 5a,b), in contrast to TCC tendency to be overestimated by COSMO models (especially in MAM). RMSE diurnal cycle is similar for both sets, with higher values at night hours.

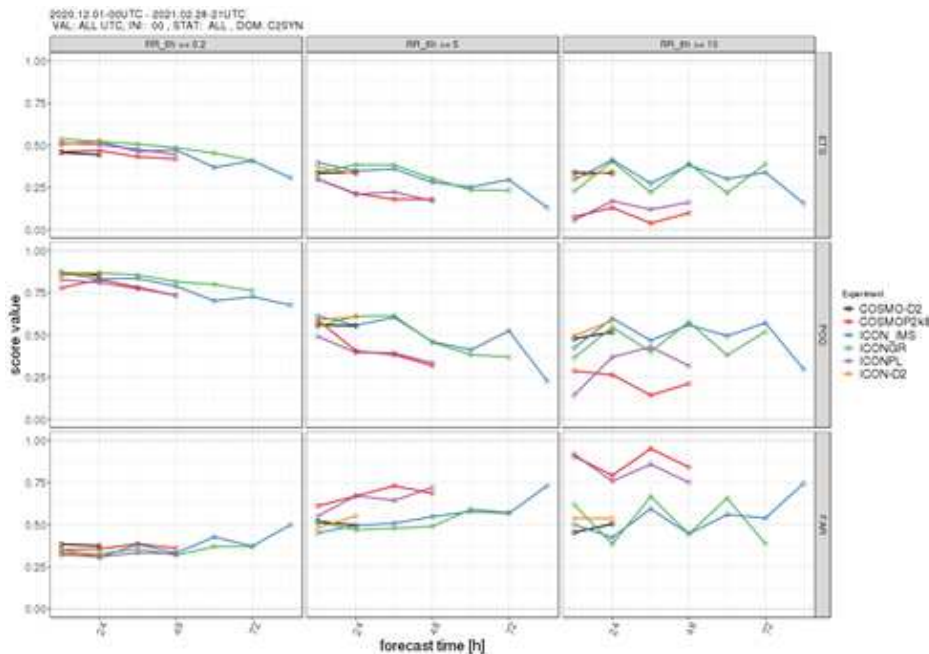


Figure 13: Precipitation scores ETS, POD, FAR (from top to bottom) for DJF2021 for thresholds 0.2,5, 10mm (from left to right) for ComA-2.

The precipitation scores for ICON and COSMO models are comparable for low thresholds, but the difference is apparent in higher thresholds. ICON-D2, ICON-GR and ICON-IMS scores are better for all indices, as it is shown in Figure 5 for DJF2021. However, ICON-PL scores which are comparable with COSMO-PL, are worse than other models, and this is result is in contrast to CM1 findings. Therefore, it cannot be extracted that ICON models outperform the COSMO for precipitation for all model configurations.

4 Fuzzy Verification Approach

In this section, fuzzy verification scores are presented for ComA-2 against the OPERA network radar composites. For this activity, VAST COSMO software is used that is based on Beth Ebert fuzzy verification IDL code. VAST main code utilizes txt gridded files for each weather parameter, but also a preprocessing of input files is available with the help of LIBSIM software. As these tools are based on grib1 format as input, while a preprocessing of ICON files needs to be performed beforehand. In the Table below, the specifications of this activity are given:

The main indices presented that summarize the spatial verification results, are the FAR (left), Fraction Skill Score (middle) and POD (right) (Fig. 6). The scores directly compare the forecast and the observation (radar) 3-hour gridded precipitation fields on continuously increasing spatial windows and for varying precipitation thresholds. The results for two different thresholds are presented in each graph, 0.1 and 5mm/3h for the first forecast day and for the three seasons (SON20, DJF21, MAM21). With spatial verification approaches, a relatively improved skill of ICON-LAM models compared to COSMO ones is shown in precipitation forecasts especially with respect to FAR and FSS scores while for POD score as also was extracted from the point-wise verification mainly for the smaller thresholds, the scores are in some cases slightly worse. The complete range of available plots of the indices can be found in: <http://www.cosmo-model.org/content/tasks/verification.priv/default.htm>.

DATA	FORMAT
Observation	OPERA composite (HDF-5) Mercator projection Resolution: 2km
Forecast	Model grib1 output format 00UTC run Horizon: up to 72h
Verification	Area: W10.97, S46.6, E17.42, N49.55

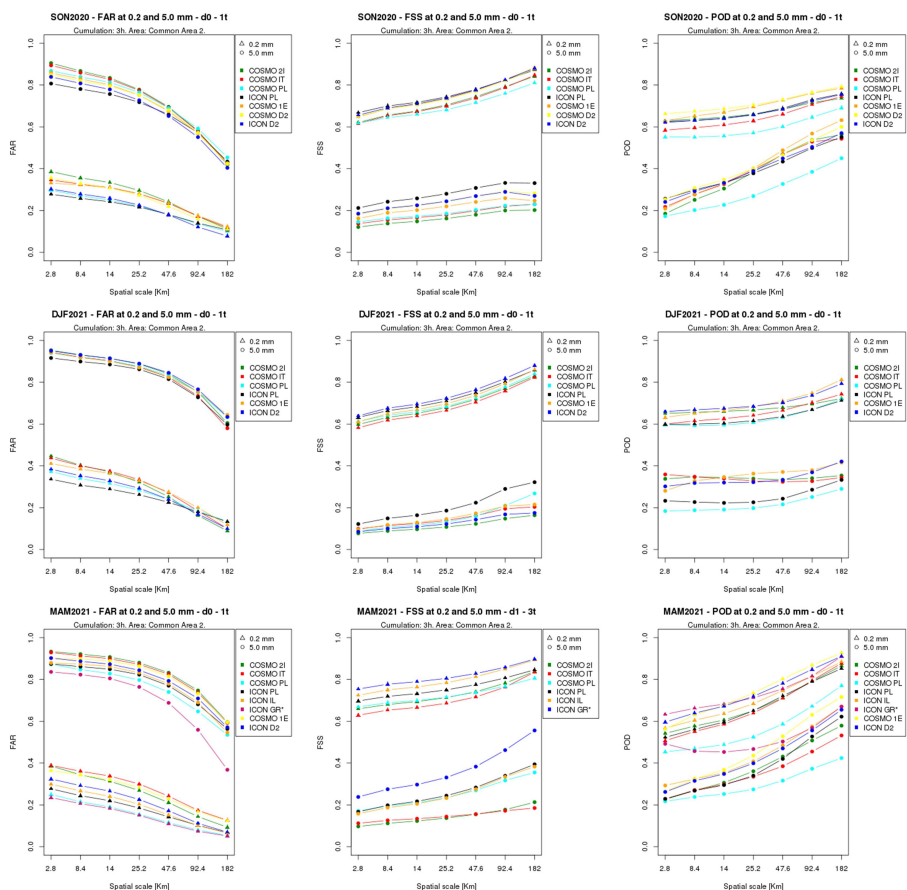


Figure 14: FAR (left), FSS (middle) and POD (right) 3h Precipitation scores for forecast day 1 (first row) for SON20 (top row), DJF21 (middle row) and MAM21 (lower row) calculated over ComA-2.

5 Main Concerns based on Common Plot Analysis

The main score trends for COSMO models have not significantly changed from previous year.

Temperature: The general tendency is to underpredict the temperature diurnal cycle especially in the summer. ICON models bias diurnal cycle is weaker and RMSE values lower.

Wind speed: The bias diurnal cycle is more pronounced for COSMO models with nighttime wind speed overprediction. On the other side, there is a tendency of constant slight wind speed underestimation for ICON models mostly found in CA1. However, some ICON fine resolution models in CA2, slightly overpredict wind speed especially in morning hours.

TCC: RMSE for all models is higher at night and lower for DJF season with COSMO and ICON values being generally on the same range. TCC is over forecasted at night especially in warm seasons. ICON models diurnal variation is weaker, in addition to a tendency of TCC underestimation which is mostly found in CA2 finer resolution models. The categorical verification showed that the error is mostly found for 25-75% and that the cases $>75\%$ are overestimated especially for COSMO models.

PS: PS bias diurnal cycle is distinct in JJA and weaker for ICON models. In DJF, ICON models slightly under forecast PS in contrast to positive bias COSMO values. RMSE increases with time with lower ICON values.

T2d: Distinct T2d overprediction in warm hours for all models especially in JJA and MAM, with respective maximal RMSE. Weaker diurnal cycle and RMSE values for ICON models.

Precipitation: The daily variation of the scores for COSMO and ICON models are similar, and stronger for warm seasons. The performance decreases with forecast time and threshold. The differences among the two sets of models are not clear for all implementations even if from the spatial approaches an improved performance of ICON-LAM models is shown based on FAR and FSS scores.

Trend from last year: By comparing the mean seasonal RMSE for each variable over the years for CM1, and for each forecast hour, ([cosmo – model.org/content/tasks/verification_priv/common/plots/default.htm](https://cosmo-model.org/content/tasks/verification_priv/common/plots/default.htm)) the tendency for all models is a general small improvement of RMSE score for T2m, Wind Speed and T2d in comparison to last year, for all seasons. Regarding TCC, although the scores are significantly better for DJF and comparable for JJA and MAM, they are worse for SON season showing a slight RMSE increase. For the same season (SON), PS RMSE values also show a slight increase, while they are comparable for the remaining seasons.

COSMO-Model 6.0 - The Last Official Version

ULRICH SCHÄTTLER

Deutscher Wetterdienst

1 Introduction

Already during the COSMO General Meeting in Eretria in 2014, one year after COSMO version 5.0 had been released, DWD announced that a limited-area mode of ICON will be developed to achieve a uniform modelling system for operational forecasting in the mid-term future. Three years later there was already clear evidence, that ICON-LAM will deliver significantly better forecasts than COSMO. This started the final phase of developments for the COSMO-Model and we put up a list of contributions for the last official version 6.0, which should be released at the end of 2019.

In this article we will summarize the activities from the last years and try to explain, why there was a delay of about two years until version 6.0 could really be published.

When starting to plan this last version in 2018, the implementation of a unified COSMO-ICON physics package just had finished with results that were not really satisfying. A deeper investigation of the differences between ICON and COSMO, which we will summarize in Section 2, strengthened the decision to only invest in the ICON-LAM from now on.

But of course the ongoing work for COSMO should be included in the last official version. The developments covered the COSMO-EULAG dynamical core and the outcomes from the priority project *Testing and Tuning the Revised Cloud-Radiation Coupling*. Also some tasks which were only about to start were added to the list of accepted contributions for 6.0, including the TERRA-URB scheme (from priority task AEVUS) and the new multi-layer snow-scheme SNOWPOLINO (from priority task SAINT). Short descriptions of these works are given in Section 3.

Besides the meteorological aspects, the results of the technical priority project *POMPA*, which ported the major parts of COSMO to GPUs, were also incorporated, which is described in Section 4.

And last, but not least, version 6.0 again is a *unified system*, which means that contributions from the CLM Community also have been taken over to the official COSMO version. The add-ons from the CLM group are listed in Section 5.

More information on all the implementation and development work can be found in the (<http://www.cosmo-model.org/content/model/releases/histories/default.htm>) [Release Notes](#) for the different versions and the pages for the priority projects and priority tasks.

2 The COSMO-ICON physics package

Between 2016 and 2018 a major restructuring of the COSMO-Model physics package has been implemented. Goal was to use the same code for the physical parameterizations like ICON, at least as far as possible. For such a unification of the physics, several issues had to be addressed:

- Memory layout, data structures

The data structure, that has been implemented in all parameterizations, is the one from ICON, a 2-dimensional one (**number of grid points, vertical dimension**), whereas the COSMO-Model uses a 3-dimensional memory layout and data structure, where horizontal fields are stored with 2 dimensions: (**ie,je, vertical dimension**). The new 2-dimensional structure is referred to as the blocked data

structure. Because the rest of the COSMO-Model still is running in the traditional ijk data structure, the data have to be copied between these two structures, to call the physical parameterizations. Fig. 1 illustrates a horizontal field in the traditional COSMO (ie, je) data structure on the left side, where all grid points are stored in a 2-dimensional array. The blocked structure is depicted on the right side with a block length of $nproma = 8$ grid points.

- Interfaces

All global fields (multidimensional arrays), which are used in a parameterization, are now passed by argument lists. All other (scalar) variables still can be accessed via `USE` statements.

- Naming conventions (of modules, routines, variables)

In COSMO and in ICON there are different naming conventions for modules and routines, but also for variables. Where possible, the names have been unified.

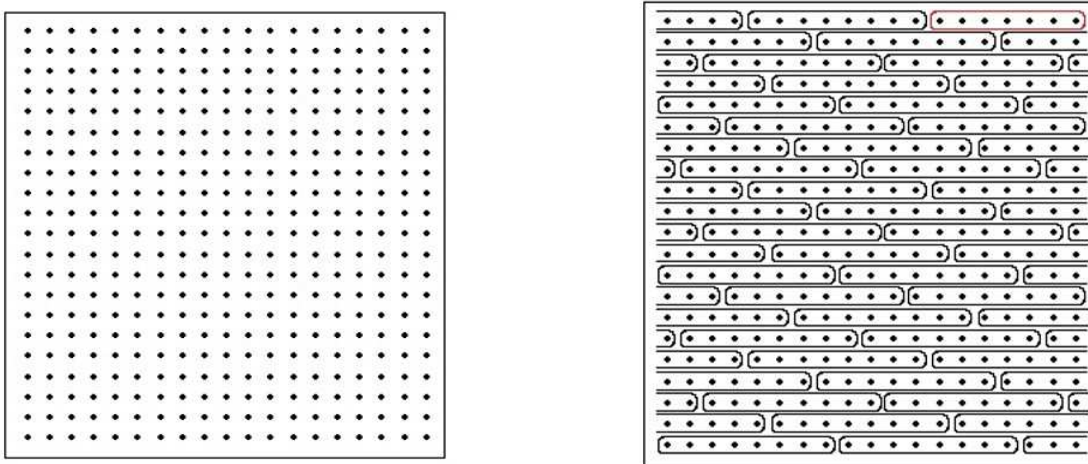


Figure 1: Horizontal field in (ie, je) (left) and blocked data structure ($nproma, nblock$) (right)

For the COSMO-ICON physics we do not store the full 3-dimensional fields. The long-term memory, to save values from one time step to another, still is in the traditional (ie, je, ke) structure. To run the physical parameterization for one step, we only copy the values for just one block to the new data structure and copy back the results to the (ie, je, ke) fields. This means, that more copy work has to be done, but less memory is consumed.

Figure 2 shows the parameterization packages used in COSMO and ICON. The ones with a blue background are not fully unified, but the scheme used is the same. All parameterizations with a green background really share the same source code with the same file names in COSMO and in ICON.

Results of using the COSMO-ICON physics in the COSMO-Model

Especially for the turbulence scheme and TERRA there have been significant modifications for the ICON implementations, that have now also been taken to COSMO. We refer to the COSMO Release Notes for version 5.04a (turbulence scheme) and 5.04e (TERRA) for further informations to these changes.

Alas, when running COSMO-DE experiments with the new versions, the results got worse compared to the former implementations. A major problem was the drying out of the soil during the simulated periods. And although COSMO was using nearly the same packages as ICON, there still were some significant differences. Among them are the treatment of external parameters, where COSMO reads *end products*, while ICON reads *raw data* and prepares them for using a tile-approach, which is not possible in COSMO. Also some parameterization components from ICON, which make direct use of land-use classes for example, cannot be transferred to COSMO.

Scheme	COSMO	ICON
Microphysics	prognostic water vapour, cloud water, ice, rain, snow, graupel (Doms, 2004; Seifert, 2010)	
Radiation	Ritter-Geleyn δ two-stream	RRTM
Subgrid scale orography	Lott and Miller (1997)	
Turbulence	prognostic TKE scheme (Raschendorfer)	
Surface Schemes	TERRA (Heise and Schrodin, 2002) FLake (Mironov) Sealce (from IFS)	
Convection	Tiedtke or shallow	
	Tiedtke-Bechtold (in COSMO only optional)	

Figure 2: Physics packages unified between COSMO and ICON

Another major difference is that ICON runs a soil-moisture analysis, which was never implemented for COSMO-DE.

Because of these results, DWD decided to run the physics schemes taken from ICON in the old "COSMO-style", which was possible by choosing a special namelist configuration. But performing and evaluating the COSMO-DE experiments took some time, which resulted in a late delivery of COSMO-Model version 5.05. And now it was clear that there was at least no easy way to further improve COSMO forecasts.

3 Meteorological Developments

Implementation of COSMO-EULAG dynamical core

The first implementations of the COSMO dynamical cores (Leapfrog and Runge-Kutta) did have no explicit conservation properties, which is a crucial issue in fluid dynamics. To implement that, a priority project CDC (Conservative Dynamical Core; 2008-2012) was started. A subtask of the project was to investigate the anelastic EULAG dynamical core regarding its use in COSMO. Two further priority projects CELO (COSMO-EULAG operationalization; 2012-2017) and EX-CELO (Extension of COSMO-EULAG operationalization; 2017-2019) were conducted to integrate the EULAG dynamical core later on into the COSMO framework and also address data assimilation issues.

During these projects, the original EULAG dynamical core changed from an anelastic to a compressible formulation, which caused some delays of the developments. In the end, the implementation in COSMO version 5.07a in May 2020 came too late for a wide-spread operational use. Moreover, improvements had also been implemented in the existing Runge-Kutta dynamical core to tackle conservation issues and the problems of steep orography.

Revised Cloud Radiation Coupling

Radiation is the main source of earth's energy and is strongly coupled to other elements of NWP models especially the heating and cooling rates. Following a Priority Task "(RC)²" (Revised Cloud Radiation Coupling), the Priority Project "T²(RC)²" (Testing and Tuning the Revised Cloud Radiation Coupling) aimed at improving the cloud-radiation coupling. For more information see the (<http://www.cosmo-model.org/content/tasks/pastProjects/t2rc2/default.htm>) [project description](#) on the COSMO Web Page.

This project started in 2015 and was finished in 2020 shortly after implementing the code extensions in the

official COSMO version 5.06b in October 2019.

TERRA-URB

The urban-canopy land-surface scheme TERRA_URB has originally been implemented in the COSMO CLM, version `cclm-sp-2.4-terra_urb-2.2.1`, and later also in the version `cclm_urb_clm9.2.3` by Hendrik Wouters. These versions still used the classical `ijk` data structure. In 2018, TERRA_URB 2.3 from this latter version has been extracted and implemented in a test version based on COSMO-Model 5.05 using the blocked data structure for the physics. Quite some technical adaptations had to be implemented because of that. The test version has been used in the priority tasks (http://www.cosmo-model.org/content/tasks/pastTasks/pt_aevus.priv.pdf) **AEVUS** and (http://www.cosmo-model.org/content/tasks/pastTasks/pt_aevus2.priv.pdf) **AEVUS2** (Analysis and Evaluation of TERRA_URB Scheme).

In 2021 this test version based on 5.05 has been finally implemented in the official COSMO version. The simple tile approach that is used in TERRA_URB for soil and surface variables needed considerable modifications in the framework of the model, especially for the I/O. While there was only a *quick and dirty* implementation in the test version, a *clean* implementation was done for COSMO version 5.09, which took some time.

A new Multi-Layer Snow Model for COSMO

The single layer snow model in TERRA has some limitations and draw-backs for numerical weather prediction, as e.g. the missing of a melting and freezing cycle. An already existing multi-layer snow model in COSMO gives better results but is not ready for operational use and is no longer developed and maintained due to lack of resources.

Here MeteoSwiss and the Swiss Institute for Snow and Avalanche Research in Davos (SLF) stepped in and started the priority task (http://www.cosmo-model.org/content/tasks/priorityTasks/pt_saint.priv.pdf) **SAINT** in 2017 to implement an improved snow model in COSMO. The task was extended a few times and was succeeded by the Working Group 3b task SNOWPOLINO in 2021.

The new snow model is essentially based on the model SNOWPACK from SLF and provides a good basis for future developments also in ICON. A first intensively tested version has been implemented in COSMO 6.0. But development is going on and the ICON version of SNOWPOLINO might already see further differences.

4 Porting the COSMO-Model to GPUs

In 2010 Switzerland started a major initiative to develop applications to run at scale and make efficient use of *next generation of supercomputers*. This initiative HP2C (Swiss Platform for High-Performance and High-Productivity Computing) has been succeeded later on by PASC, the Swiss Platform for Advanced Scientific Computing. Within these initiatives also projects were started to make the COSMO-Model aware of these emerging massively parallel computers. The COSMO priority project (<http://www.cosmo-model.org/content/tasks/pastProjects/pompa/default.htm>) **POMPA** (Performance on Massively Parallel Architectures; 2010-2015) supported these swiss initiatives.

The target architecture for POMPA were general purpose graphic cards (GP-GPUs), which need a different way of programming compared to CPUs. For the dynamical core, a rewrite using a domain specific language (DSL) has been chosen. The first prototype of the DSL called STELLA (stencil library) has been replaced some time ago by GRIDTOOLS. All other components of COSMO have been ported by adding OpenACC compiler directives to the Fortran code, which can be processed by a few compilers.

Another outcome of POMPA was a running single-precision version. To run the COSMO-Model in single precision has been aimed at from the very beginning of the development, but has never been tested. Therefore

it was a major achievement to make this work.

COSMO version 5.07 was the first in which all components were ported to GPUs, which are used at MeteoSwiss and the Aeronautica Militare in Rome, who are running GPU systems.

5 Unification with CLM Versions

A goal for every major version of COSMO always was the re-unification with the code used in the CLM Community, the COSMO-CLM. This also was planned again for version 6.0. This time we got contributions from the COSMO-CLM, but also from the C2SM (Center for Climate Systems Modelling) group at the ETH in Zürich. Most of these developments have been implemented in version 5.08, unless stated otherwise.

Contributions from CLM

The CLM Community added several diagnostic output variables, for example for wind sector classes and for sunshine duration. Also new tuning variables have been introduced for several parameterization schemes.

In the module `src_setup_vartab.f90` only official NetCDF standard and long names are now used. Some of these names have been explicitly registered by the NetCDF community. If no official names exist, only a '-' appears (version 5.09b).

Contributions from C2SM

A new additional hydrology scheme (groundwater and runoff) has been developed by Linda Schlemmer during her stay at the ETH. This has been implemented in COSMO version 5.08. For this scheme and also for the radiation some additional diagnostic output variables have been added.

Colleagues from the ETH also worked on NetCDF I/O. In the last years they were using a COSMO version based on the work done at MeteoSwiss to run the model on GPUs. And because they are using a rather powerful GPU machine, they can run very big COSMO domains, which showed some limitations in NetCDF I/O. To overcome at least some of these limitations, a prefetching of NetCDF boundary data has been implemented (version 5.11) and some optimizations for asynchronous output have been done (version 5.09). And because classic NetCDF restricts the size of variables the possibility to work with NetCDF4 is available (version 5.09). Also, an online compression of NetCDF data using zlib can now be done (version 5.10).

Together with colleagues from the CLM group also the possibility to write restart files in NetCDF has been implemented (version 5.06b).

Contributions from MESSy

The interfaces to couple MESSy packages with COSMO and INT2LM have been updated. The MESSy group regularly is testing COSMO and INT2LM with the NAG Compiler (Numerical Algorithms Group), which does a very thorough testing of the Fortran Standard. Because of that we got several updates from the MESSy group to improve our codes.

One major contribution was the implementation of some MPI 3.0 interfaces, where the names and / or the functionality had changed. For COSMO the module `environment.f90` was affected, where MPI data types are used. The new interfaces are implemented with a `pragma MPI3`, and the old interfaces are retained for installations, which do not yet provide MPI 3.0 standard.

6 Summary

For more than 20 years the COSMO-Model served as an operational forecast model not only at DWD, but at about 30 national weather centers. Also it was used as a regional climate model by the CLM Community and as a research tool at numerous institutions worldwide.

We would like to thank all the users who contributed to the development and the improvement of the code

and the documentation of the COSMO-Model in these two decades. It sure was an outstanding experience working together with all of you!

On 10th of February, 2021, DWD replaced its COSMO-D2 with the application ICON-D2, based on the limited-area mode of ICON. With that, no more COSMO application is now running at DWD. Nevertheless, all other partners still are using the COSMO-Model. While the consortium partners already started to migrate their work also to ICON-LAM, all other partners as the licensees or the CLM community may stay with COSMO for a bit longer. Therefore, support and maintenance for running the COSMO-Model still is ongoing, but there will be no more further developments. Maintenance now is limited to bug-fixes only.

With that we invite all of you to use the ICON-LAM in the future and start to migrate your work now.

Farewell to COSMO

Welcome to and Good Luck with ICON-LAM

Priority Project COSMO-EULAG Operationalization (PP CELO)

BOGDAN ROSA¹, MARCIN J. KUROWSKI², JOANNA LINKOWSKA¹, ZBIGNIEW P. PIOTROWSKI¹, DAMIAN K. WÓJCIK¹ AND MICHAŁ Z. ZIEMIAŃSKI¹

1 Instytut Meteorologii i Gospodarki Wodnej - PIB, Warsaw, Poland

2 Jet Propulsion Laboratory, California Institute of Technology, Pasadena, California

1 Introduction

The progress in the convective-scale numerical weather prediction (NWP) at the beginning of 2000s motivated the COSMO Consortium to discuss and formulate an optimal model development strategy to address new challenges emerging at those scales. The strategy was formulated in the COSMO Science Plan (Arpagaus et al. 2010), which for dynamics called for high accuracy, numerical robustness and computational efficiency. Specifically, the Science Plan pointed at potential advantages of conservative properties of prospective future dynamical core in dealing with steep gradients and discontinuities (Le Veque 2003). Following the strategy, the COSMO Priority Project Conservative Dynamical Core (PP CDC) considered, in between, a conservative version of an already existing anelastic EULAG research dynamical core (Prusa et al. 2008) as a potential candidate for the new dynamical core of the operational COSMO model.

The PP CDC proved that the anelastic EULAG dynamical core is a feasible candidate for the purpose. The successful results of the core's numerous tests for a range of idealized and semi-realistic flows and new developing super-computer architectures were published by Rosa et al. (2011), Kurowski et al. (2011), Piotrowski et al. (2011), Ziemiański et al. (2011) and Baldauf et al. (2013).

Consequently, PP CDC was followed by the Priority Project COSMO-EULAG Operationalization (PP CELO), aiming to fully integrate of the EULAG dynamical core with the COSMO framework. The project work involved consolidation and optimization of the setup of the dynamical core for the high-resolution NWP, coupling with the COSMO physical parameterizations. The work was further followed by testing and exploiting the forecasting capabilities of the new integrated model: the COSMO-EULAG (CE). This article briefly summarizes the development and results of PP CELO.

2 Some Formulas

Following the PP CELO project plan, the work considered at first the implementation of the anelastic version of the EULAG dynamical core (based on the soundproof atmospheric equations of Lipps and Hemmler 1982) within the COSMO model framework. The successful results of that part of the project are documented mainly in (Kurowski et al. 2016). In the meantime, the fully compressible semi-implicit version of the EULAG dynamical core was developed (Smolarkiewicz et al. 2014 and 2016, Kurowski et al. 2014, 2015). Following that development, the Consortium decided to extend the project plan to implement the new compressible version of EULAG as the dynamical core of the COSMO model. The successful results of that work are documented in Ziemiański et al. (2021), together with the results of the Priority Task Consolidation of COSMO-EULAG (PT CCE), which followed PP CELO and which results are summarised in the companion article (Wójcik et al. 2021). The work within PP CELO was structured within five main project tasks, which are briefly discussed below.

doi:10.5676/dwd-pub/nwv/cosmo-nl_21_07

2.1 The integration of EULAG dynamical core with COSMO framework

Within this task, the EULAG dynamical core was re-configured to optimize the coupling with the COSMO environment. Also, a coupler between the core and the COSMO model infrastructure was constructed to account for the different native grid structures: A-grid for EULAG and C-grid for COSMO, and different prognostic variables of the Runge-Kutta and EULAG cores. The coupler allows for the communication between the dynamical core and physical parameterizations and the use of native COSMO initialization and I/O procedures. Also, it allows for EULAG physics-dynamics coupling equivalent to the integration of forcings along the flow trajectory. Two different configurations of the dynamical core were prepared and tested: first with additional EULAG mass level on the ground for a provision of the same boundary condition for vertical velocity there (finally implemented in the anelastic model version). The second configuration was without that additional level (finally implemented in the compressible version of the model), with all EULAG mass levels and points as in the Runge-Kutta dynamical core configuration.

The work needed to account for the ongoing development of the mother COSMO model. The task started with implementing EULAG into model version 4.26 and needed to follow the subsequent developments of COSMO physical parameterizations in their ongoing unification with the ICON parameterizations. Currently, the EULAG dynamical core is implemented into COSMO 6.0. The correctness of the EULAG setup and the coupler were extensively tested during the development work against the idealised benchmark experiments with moist convective flows: the supercell of Weisman and Klemp (1982) and the daytime convective development of Grabowski et al. (2006). They proved to be very useful for the task and were applied using varying horizontal resolutions. Finally, the dynamical core configuration and the coupler were extensively and successfully tested for real convective and non-convective weather forecasts, especially over the Alpine domain.

2.2 Consolidation and optimization of the formulation of the Eulag dynamical core

As the anelastic dynamical core provides information on pressure perturbations, the problem of recovering of the full pressure from the anelastic system was analysed. The idealized experiments have shown that the anelastic pressure perturbations are comparable with their compressible analogs (Kurowski et al. 2013) while Kurowski et al. (2016) have shown for realistic flows that moist processes are weakly sensitive to various alternative methods of full pressure recovery and used the time-dependent pressure from the driving model.

Further work concerned a consistent formulation of the dynamical core for different versions of the vertical coordinates, handled by the COSMO model options, and a correct implementation of the boundary conditions for the advection operator MPDATA, consistent with the anelastic integrability condition. In addition, an alternative preconditioner for the solution of the elliptic pressure equation was developed, implemented, and tested (Piotrowski et al. 2016).

2.3 Eulag DC code restructuring and engineering

The task was focused on the optimization and further consolidation/integration of the EULAG dynamical core with the COSMO numerical framework. Its code was restructured for a more transparent exposition of its algorithmic foundation, optimized for minimizing the need for communication and overlapping of communication and computation. In addition, flexible parallelization subdomains were implemented and tested.

Further work concerned an assessment of the feasibility of transforming the EULAG code into a stencil library in the context of potential code adaptations to the emerging computer architectures. The work included porting of EULAG dynamical core and especially its crucial MPDATA and iterative elliptic solver procedures to GPU and MIC architectures. The results show a potential speedup that can be achieved on modern architectures and were published in several articles: (Rosa et al. 2014 and 2015), and (Rojek et al. 2015).

2.4 Optimization and testing of COSMO with EULAG dynamical core

The finally developed CE was thoroughly tested for its anelastic and compressible versions. At first, the tests involved moist idealized flows (Weisman and Klemp 1982, and Grabowski et al. 2006) followed by realistic weather simulations. The model was tested for different horizontal resolutions with grid sizes ranging between 2.2 and 0.1 km. The sensitivity of model solutions to different values of tunable parameters of physical parameterizations was tested. For convective flows, a strong sensitivity was found for the varying turbulent diffusivity of the model. Also, different microphysical setups were tested, from a rain scheme to a more complicated setup involving a groupel presence. The majority of advanced experiments for realistic weather were performed for realistic Alpine domains to provide a demanding environment for testing model numerical robustness and physics-dynamics coupling. The tests involved both analyses of case studies and more extended periods for standard verification studies.

2.5 Integration and consolidation of the EULAG compressible DC with COSMO framework

The task was added to the project plan after the anelastic version of the CE was developed. The semi-implicit compressible EULAG dynamical core was integrated with the COSMO framework. The main work in this task involved an introduction of two-level density and pressure as new prognostic variables throughout the code, new formulations for ambient profiles (including ambient pressure and density) and appropriate boundary conditions, and extending the existing elliptic solver formulation for new Helmholtz operators and custom preconditioner. In general, the compressible variables add considerable complexity to the model formulation. This development aims at convective-scale NWP regional applications and, as such, supplements the ECMWF studies on the implementation of the semi-implicit compressible EULAG for global applications within the Finite Volume Module of IFS (Kühnlein et al. 2019).

Before the compressible CE was tested for moist flows and realistic weather scenerios, as described in section 2.4, it was first successfully tested for standard benchmark idealized experiments including cold density currents (Straka et al. 1993), inertia-gravity waves (Skamarock and Klemp 2004), and mountain flows (e.g., Bonaventura 2000). In view of potential future applications in diverse High Performance Computing environments, the dynamical core was tested on a variety of standard compilers used for CPU architectures.

3 Conclusion

The project delivered its main expected result: the fully-operational COSMO-EULAG weather prediction package, without data assimilation, for two variants of the dynamical core: anelastic and semi-implicit compressible. Furthermore, as shown by Kurowski et al. (2016) and Ziemiański et al. (2021), the COSMO-EULAG is numerically stable over Alpine domains even for very high resolutions. Its verification results are similar or competitive when compared to the standard COSMO model employing the Runge-Kutta dynamical core.

Acknowledgments

Support of Piotr Smolarkiewicz and Wojciech Grabowski in the development of COSMO-EULAG is gratefully acknowledged. The implementation of the compressible EULAG benefitted from the exchange of ideas with ECMWF's group working on the Finite Volume Module of IFS. We acknowledge the help of MeteoSwiss in providing initial and boundary conditions for realistic weather simulations and observational data for verification studies. The computational resources were partly provided by the Swiss National Supercomputing Centre (CSCS) under ID d25 and PRACE projects.

References

- [1] Arpagaus, M., H. Asensio, M. Baldauf, J.-M. Bettems, U. Blahak, P. Eckert, F. Grazzini, J. Helmert, H.-J. Koppert, D. Majewski, C. Marsigli, D. Mironow, R. Potthast, M. Raschendorfer, A. Raspanti, B. Ritter, M. W. Rotach, U. Schättler, C. Schraff, F. Schubiger, A. Seifert and S. Theis, 2010: COSMO Science Plan 2010-2014, Consortium for Small-scale Modeling, 79pp, www.cosmo-model.org/content/consortium/reports/sciencePlan_2010-2014.pdf
- [2] Baldauf, M., O. Fuhrer, M. J. Kurowski, G. de Morsier, M. Muellner, Z. P. Piotrowski, B. Rosa, P. L. Vitagliano, D. K. Wójcik and M. Z. Ziemiański, 2013: The COSMO Priority Project Conservative Dynamical Core Final Report, Consortium for Small-scale Modeling, 118pp, https://doi.org/10.5676/DWD_pub/nwv/cosmo-tr_23.
- [3] Bonaventura, L., 2000: A semi-implicit semi-Lagrangian scheme using the height coordinate for a nonhydrostatic and fully elastic model of atmospheric flows, *J. Comput. Phys.*, 152, **186–213**, <https://doi.org/10.1006/jcph.1999.6414>.
- [4] Grabowski, W. W., P. Bechtold, A. Cheng, R. Forbes, C. Halliwell, M. Khairoutdinov, S. Lang, T. Nansuno, J. Petch, W.-K. Tao, R. Wong, X. Wu, K.-M. Xu, 2006: Daytime convective development over land: A model intercomparison based on LBA observations, *Quart. J. Roy. Meteor. Soc.*, 132, **317–344**, <https://doi.org/10.1256/qj.04.147>.
- [5] Kurowski, M. J., B. Rosa and M. Z. Ziemiański, 2011: Testing the anelastic nonhydrostatic model EULAG as a prospective dynamical core of a numerical weather prediction model. Part II: Simulations of supercell, *Acta Geophys.*, 59, **1267–1293**, <https://doi.org/10.2478/s11600-011-0051-z>.
- [6] Kurowski, M. J., W. W. Grabowski and P. K. Smolarkiewicz, 2013: Toward multiscale simulation of moist flow with soundproof equations, *J. Atmos. Sci.*, 70, **3995–4011**, <https://doi.org/10.1175/JAS-D-13-024.1>.
- [7] Kurowski, M. J., P. K. Smolarkiewicz and W. W. Grabowski, 2014: Anelastic and Compressible Simulations of Moist Deep Convection, *J. Atmos. Sci.*, 71, **3767–3787**, <https://doi.org/10.1175/JAS-D-14-0017.1>.
- [8] Kurowski, M. J., D. K. Wójcik, M. Z. Ziemiański, B. Rosa and Z. P. Piotrowski, 2016: Convection-Permitting Regional Weather Modeling with COSMO-EULAG: Compressible and Anelastic Solutions for a typical Westerly Flow over the Alps, *Mon. Wea. Rev.*, 144, **1961–1982**, <https://doi.org/10.1175/MWR-D-15-0264.1>.
- [9] Kühnlein, C., W. Deconinck, R. Klein, S. Malardel, Z. P. Piotrowski, P. K. Smolarkiewicz, J. Szmelter and N. P. Wedi, 2019: FVM 1.0: a nonhydrostatic finite-volume dynamical core for IFS, *Geosci. Model Dev.*, 12, **651–676**, <https://doi.org/10.5194/gmd-12-651-2019>
- [10] LeVeque, R. J., 2002: Finite Volume Methods for Hyperbolic Problems, *Cambridge University Press*, pp. **580**
- [11] Lipps, F.B. and R.S. Hemler, 1982: A scale analysis of deep moist convection and some related numerical calculations, *J. Atmos. Sci.*, 39, **2192–2210**, [https://doi.org/10.1175/1520-0469\(1982\)039<2192:ASAODM>2.0.CO;2](https://doi.org/10.1175/1520-0469(1982)039<2192:ASAODM>2.0.CO;2).
- [12] Piotrowski, Z. P., A. A. Wyszogrodzki and P. K. Smolarkiewicz, 2011: Towards petascale simulation of atmospheric circulation with soundproof equations, *Acta Geophys.*, 59, **1294–1311**, <https://doi.org/10.2478/s11600-011-0049-6>.
- [13] Piotrowski, Z. P., B. Matejczyk, L. Marcinkowski and P. K. Smolarkiewicz, 2016: Parallel ADI Preconditioners for All-Scale Atmospheric Models, In: *Wyrzykowski R., Deelman E., Dongarra J., Karczewski K., Kitowski J., Wiatr K. (eds) Parallel Processing and Applied Mathematics. Lecture Notes in Computer Science*, vol 9574. Springer, Cham. https://doi.org/10.1007/978-3-319-32152-3_56.

- [14] Prusa, J. M., P. K. Smolarkiewicz and A. A. Wyszogrodzki, 2008: EULAG, a computational model for multiscale flows, *Computers and Fluids*, 37, **1193–1207**, <https://doi.org/10.1016/j.compfluid.2007.12.001>.
- [15] Rojek, A. and Coauthors, 2015: Adaptation of fluid model EULAG to graphics processing unit architecture, *Concurr. Comput.*, 27, **937–957**, <https://doi.org/10.1002/cpe.3417>.
- [16] Rosa, B., M. J. Kurowski and M. Z. Ziemiański, 2011: Testing the anelastic nonhydrostatic model EULAG as a prospective dynamical core of a numerical weather prediction model. Part I: Dry benchmarks, *Acta Geophys.*, 59, **1236–1266**, <https://doi.org/10.2478/s11600-011-0041-1>.
- [17] Rosa, B., M. Ciznicki, A. Rojek, D. K. Wójcik, P. K. Smolarkiewicz and R. Wyrzykowski, 2014: Porting multiscale fluid model EULAG to modern heterogenous architectures, *Int. J. Appl. Phys. Math.*, 4, **188–195**, <https://doi.org/10.7763/IJAPM.2014.V4.281>.
- [18] Rosa, B., L. Szustak, A. A. Wyszogrodzki, A. Rojek, D. K. Wójcik and R. Wyrzykowski, 2015: Adaptation of Multidimensional Positive Definite Advection Transport Algorithm to modern high-performance computing platforms, *Int. J. Model. Optim.*, 5, **171–176**, <https://doi.org/10.7763/IJMO.2015.V5.456>.
- [19] Skamarock, W. C. and J. B. Klemp, 1994: Efficiency and accuracy of the Klemp-Wilhelmson time-splitting technique, *Mon. Wea. Rev.*, 122, **2623–2630**, [https://doi.org/10.1175/1520-0493\(1994\)122;2623:EAAOTK;2.0.CO;2](https://doi.org/10.1175/1520-0493(1994)122;2623:EAAOTK;2.0.CO;2).
- [20] Smolarkiewicz, P. K., C. Kühnlein and N. P. Wedi, 2014: A consistent framework for discrete integrations of soundproof and compressible PDEs of atmospheric dynamics, *J. Comput. Phys.*, 263, **185–205**, <https://doi.org/10.1016/j.jcp.2014.01.031>.
- [21] Smolarkiewicz, P. K., W. Deconinck, M. Hamrud, C. Kühnlein, G. Mozdzyński, J. Szmelter and N. P. Wedi, 2016: A finite-volume module for simulating global all-scale atmospheric flows, *J. Comput. Phys.*, 314, **287–304**, <https://doi.org/10.1016/j.jcp.2016.03.015>.
- [22] Straka, J. M., R. B. Wilhelmson, L. J. Wicker, J. R. Anderson, K. K. Droegemeier, 1993: Numerical solutions of non-linear density current: A benchmark solution and comparison, *Int. J. Numer. Methods Fluids*, 17, **1–22**, <https://doi.org/10.1002/flid.1650170103>.
- [23] Weisman, M. L. and J. B. Klemp, 1982: The dependence of numerically simulated convective storms on vertical wind shear and buoyancy, *Mon. Wea. Rev.*, 110, **504–520**, [https://doi.org/10.1175/1520-0493\(1982\)110;0504:TDONSC;2.0.CO;2](https://doi.org/10.1175/1520-0493(1982)110;0504:TDONSC;2.0.CO;2).
- [24] Wójcik, D. K., B. Rosa and M. Z. Ziemiański, 2021: Priority Task Consolidation of COSMO-EULAG, *COSMO Newsletter*, 21, **xx–xx**, <https://doi.org/xxxx.xxx.xxx>
- [25] Ziemiański, M. Z., M. J. Kurowski, Z. P. Piotrowski, B. Rosa and O. Fuhrer, 2011: Toward very high resolution NWP over the Alps: Influence of increasing model resolution on the flow pattern, *Acta Geophys.*, 59, **1205–1235**, <https://doi.org/10.2478/s11600-011-0054-9>.
- [26] Ziemiański, M. Z., D. K. Wójcik, B. Rosa, Z. P. Piotrowski, 2021: Compressible EULAG dynamical core in COSMO: convective-scale Alpine weather forecast, *Mon. Wea. Rev.*, 149, **3563–3583**, <https://doi.org/10.1175/MWR-D-20-0317.1>.

Priority Task Consolidation of COSMO-EULAG (PT CCE)

DAMIAN K. WÓJCIK¹, BOGDAN ROSA¹ AND MICHAŁ Z. ZIEMIAŃSKI¹

1 Instytut Meteorologii i Gospodarki Wodnej - PIB, Warsaw, Poland

1 Introduction and motivation

The Priority Project COSMO-EULAG Operationalization (PP CELO), discussed in a companion article (Rosa et al. 2021), ended with an implementation of the EULAG dynamical core (Prusa et al. 2008) into the COSMO model infrastructure. The resulting COSMO-EULAG (CE) model using anelastic EULAG dynamical cores was presented by Kurowski et al. (2016), and the CE model using semi-implicit compressible EULAG dynamical core was presented by Ziemiański et al. (2021). During the final stage of the Project, the compressible CE was thoroughly and successfully tested for a range of idealized and realistic experiments. The tests involved, in between, realistic simulations of Alpine convective weather with horizontal grid steps varying from 2.2 to 0.1 km. Finally, the Project merged the compressible EULAG dynamical core with the COSMO model version 5.04h.

In the meantime, a new COSMO Runge-Kutta model version 5.05 was developed. It fully integrated the ICON physical parameterizations and was intended to serve as a basic COSMO model version for future developments. Therefore, a new Priority Task Consolidation of COSMO-EULAG (PT CCE; COSMO year 2018/2019) was established to build on the results of PP CELO. The Task goal was to prepare a consolidated version of COSMO-EULAG consistent with the standard COSMO Runge-Kutta V.5.05 and provide it to the Consortium to merge with the main model trunk.

Implementation of data assimilation functionality to the CE was not anticipated within the PP CELO. However, preliminary tests showed that implementation of COSMO nudging functionality to the CE should be relatively straightforward. Therefore, it was proposed that the consolidated version of COSMO-EULAG based on COSMO V5.05 provides the nudging capability. The intention was to provide better consistency with the default COSMO Runge-Kutta code and offer better operational capabilities of the COSMO-EULAG.

It was also important to optimize the performance of CE, including its general consistency and computational aspects. It was decided to explore the additional potential for improvement from ensuring the CE procedures' full physical and dynamical consistency. At the end of PP CELO, the native EULAG MPDATA advection was used to all model variables except turbulent kinetic energy (TKE) applied in the prognostic turbulence scheme (Raschendorfer 2001). For the TKE advection, the COSMO native Bott scheme (Bott 1989) was used. The resulting lack of consistency could influence the model performance, for example, via a generation of non-physical atmospheric currents. It was decided, therefore, to implement the MPDATA also for the TKE advection in the CE.

The intended work on optimization of the CE code included improving the zero gradient boundary conditions for precipitating variables and further streamlining the code together with removing unnecessary features, and full implementation of COSMO coding standards.

This article briefly summarizes the results of the PT CCE.

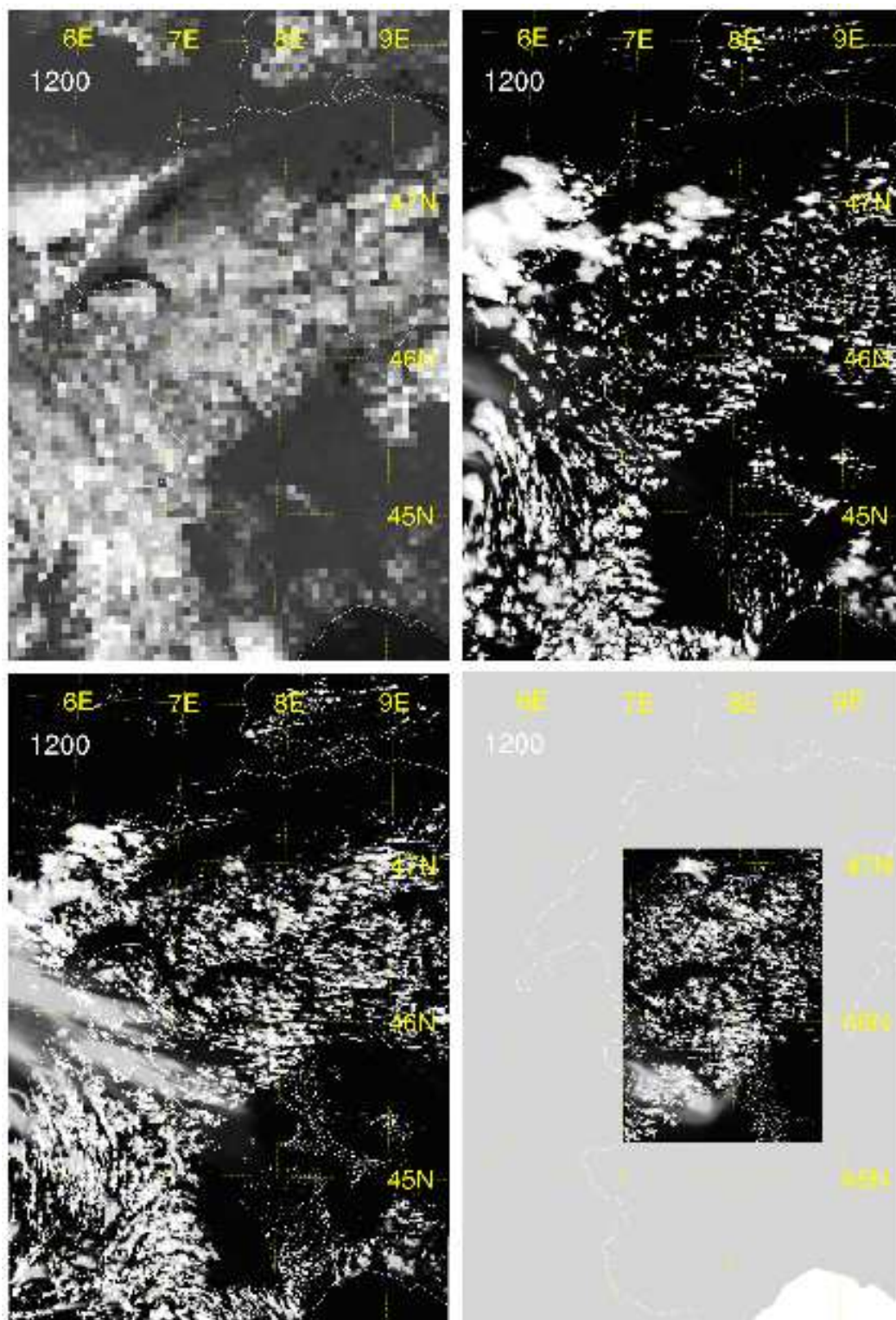


Figure 1: Cloud field over the Alps at 1200 UTC on 19 July 2013 from the Meteosat HRV observation of EUMETSAT (top left) and from the CE simulations with horizontal grid size of 1.1 km (top right), 0.22 km (bottom left), and 0.1 km (bottom right). The model clouds are represented by vertically integrated condensate including cloud water, ice, snow, and graupel

2 The Task results

The PT CCE successfully implemented the semi-implicit compressible EULAG dynamical core into the COSMO model version 5.05. The performance of that CE version is discussed in Ziemiański et al. (2021). The work within the Task was organized in two main subtasks. They are briefly reviewed below.

2.1 Provision of COSMO-EULAG based on COSMO 5.05

The EULAG compressible dynamical core was implemented within this subtask into the computational framework of COSMO version 5.05 and merged with the complete ICON physics package. That CE was extensively tested for weather simulations over the Alpine domain with horizontal grid sizes from 2.2 to 0.1 km and verified against observations. Figure 1 demonstrates the CE forecasts of convective cloud field over the Alps at 1200 UTC on 19 July 2013, performed at different resolutions, and compares them with the Meteosat HRV observations. The figure shows that with the increasing resolution, the density of the cloud field increases in better agreement with the satellite observations. Figure 2 demonstrates the CE forecasts of the vertical velocity over the Rhone Valley (see Ziemiański et al. 2021 for the details of the cross-section location) on the same day at 0900, 1200, and 1500 UTC made with horizontal grids of 1.1 and 0.1 km. The increased resolution allows for a more realistic representation of the mountain flow.

Further work within the subtask included implementation of the nudging capability. It was successfully tested over the Polish operational domain (horizontal grid size 2.8 km). Additionally, an exact restart capability was implemented into the CE and tested using the COSMO Technical Testsuite.

2.2 Improved consistency of COSMO-EULAG

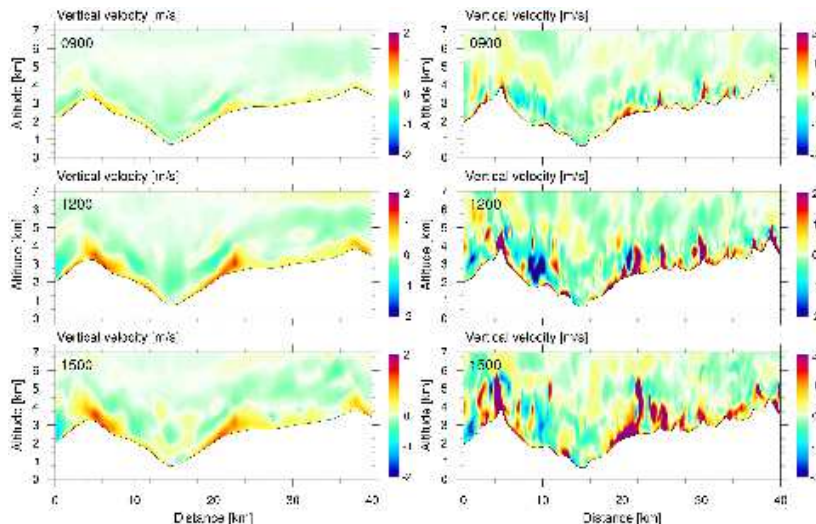


Figure 2: Vertical cross section through the vertical velocity over the Rhone Valley between Bietschhorn (left) and Weisshorn (right) on 19 July 2013 at 0900 (top row), 1200 (middle row) and 1500 UTC (bottom row). The CE forecasts with horizontal grid size of 1.1 km (left) and 0.1 km (right) are shown.

All additional functionalities expected by the Task plan were successfully implemented into the COSMO-EULAG, and the updated code was tested within the scope of subtask 1. The changes concerned the replacement of the Bott scheme by MPDATA for the TKE advection, the implementation of the zero-gradient boundary condition for the precipitating variables, and code cleaning and streamlining. The latter included a revival of the halo equal 1 code option (initially implemented in PP CELO) and a revision of the dycore loops vectorization in the X-direction. That resulted in a 20% speedup of the code execution time.

Further work involved implementing the exact (non-linearised) form of the moist buoyancy term and finalizing the scientific and user documentation of the code. Potential operational applications of the code suggested an additional study on the optimum configuration of the MPDATA advection scheme. The scheme has two options for transporting the model variables of varying signs: basic (Smolarkiewicz and Margolin 1998) and gauge (Smolarkiewicz and Clark 1986). It was shown (see Ziemiański et al. 2021) that for realistic weather simulations, the basic scheme gives generally better verification scores and is suggested for operational use within the CE.

The final version of the COSMO-EULAG model provides also support for the Smagorinsky turbulent diffusion (`itype_turb=7`), including the TKE advection by the MPDATA.

3 Conclusion

The PT CCE delivered the operational semi-implicit compressible COSMO-EULAG based on COSMO version 5.05 with the ICON physics parameterizations and a nudging assimilation package. In addition, the model code was consolidated and streamlined for better performance, and the restart procedure allows for its use for long-term simulations. Furthermore, the optimum configuration of the advection scheme for the NWP application of the model was found.

The final version of the COSMO-EULAG model is available in the main model trunk since the COSMO model version 5.08.

Acknowledgments

We acknowledge the help of MeteoSwiss in providing initial and boundary conditions for realistic weather simulations and observational data for verification studies. Figures were prepared using NCL software developed in NCAR.

References

- [1] Bott, A., 1989: A positive definite advection scheme obtained by nonlinear renormalization of the advective fluxes, *Mon. Wea. Rev.*, 117, **1006–1015**, [https://doi.org/10.1175/1520-0493\(1989\)117;1006:APDASO;2.0.CO;2](https://doi.org/10.1175/1520-0493(1989)117;1006:APDASO;2.0.CO;2).
- [2] Kurowski, M. J., D. K. Wójcik, M. Z. Ziemiański, B. Rosa and Z. P. Piotrowski, 2016: Convection-Permitting Regional Weather Modeling with COSMO-EULAG: Compressible and Anelastic Solutions for a typical Westerly Flow over the Alps, *Mon. Wea. Rev.*, 144, **1961–1982**, <https://doi.org/10.1175/MWR-D-15-0264.1>.
- [3] Prusa, J. M., P. K. Smolarkiewicz and A. A. Wyszogrodzki, 2008: EULAG, a computational model for multiscale flows, *Computers and Fluids*, 37, **1193–1207**, <https://doi.org/10.1016/j.compfluid.2007.12.001>.
- [4] Raschendorfer, M., 2001: The new turbulence parameterization of LM, *Cosmo Newsletter*, 1, **89–98**
- [5] Rosa, B., M. J. Kurowski, J. Linkowska, Z. P. Piotrowski, D. K. Wójcik, M. Z. Ziemiański, 2021: Priority Project COSMO-EULAG Operationalization, *COSMO Newsletter*, 21, **xx–xx**, <https://doi.org/xxxx.xxxx.xxxx>
- [6] Smolarkiewicz, P. K. and T. L. Clark, 1986: The multidimensional positive definite advection transport algorithm: Further development and applications, *J. Comput. Phys.*, 67, **396–438**, [https://doi.org/10.1016/0021-9991\(86\)90270-6](https://doi.org/10.1016/0021-9991(86)90270-6).

-
- [7] Smolarkiewicz, P. K. and L. G. Margolin, 1998: MPDATA: A Finite-Difference Solver for Geophysical Flows, *J. Comput. Phys.*, 140, **459–480**, <https://doi.org/10.1006/jcph.1998.5901>.
- [8] Ziemiański, M. Z., D. K. Wójcik, B. Rosa, Z. P. Piotrowski, 2021: Compressible EULAG dynamical core in COSMO: convective-scale Alpine weather forecast, *Mon. Wea. Rev.*, 149, **3563–3583**, <https://doi.org/10.1175/MWR-D-20-0317.1>.

List of COSMO Newsletters and Technical Reports

(available for download from the COSMO Website: www.cosmo-model.org)

COSMO Newsletters

- No. 1: February 2001.
- No. 2: February 2002.
- No. 3: February 2003.
- No. 4: February 2004.
- No. 5: April 2005.
- No. 6: July 2006; Proceedings from the COSMO General Meeting 2005.
- No. 7: May 2008; Proceedings from the COSMO General Meeting 2006.
- No. 8: August 2008; Proceedings from the COSMO General Meeting 2007.
- No. 9: December 2008; Proceedings from the COSMO General Meeting 2008.
- No.10: January 2010; Proceedings from the COSMO General Meeting 2009.
- No.11: February 2011; Proceedings from the COSMO General Meeting 2010.
- No.12: March 2012; Proceedings from the COSMO General Meeting 2011.
- No.13: April 2013; Proceedings from the COSMO General Meeting 2012.
- No.14: April 2014; Proceedings from the COSMO General Meeting 2013.
- No.15: July 2015; Proceedings from the COSMO General Meeting 2014.
- No.16: June 2016; Proceedings from the COSMO General Meeting 2015.
- No.17: July 2017; Proceedings from the COSMO General Meeting 2016.
- No.18: November 2018; Proceedings from the COSMO General Meeting 2017.
- No.19: October 2019; Proceedings from the COSMO General Meeting 2018.
- No.20: November 2020; Proceedings from the COSMO General Meeting 2019.
- No.21: May 2022; Proceedings from the COSMO General Meeting 2021.

COSMO Technical Reports

- No. 1: Dmitrii Mironov and Matthias Raschendorfer (2001):
Evaluation of Empirical Parameters of the New LM Surface-Layer Parameterization Scheme. Results from Numerical Experiments Including the Soil Moisture Analysis.
- No. 2: Reinhold Schrodin and Erdmann Heise (2001):
The Multi-Layer Version of the DWD Soil Model TERRA_LM.
- No. 3: Günther Doms (2001):
A Scheme for Monotonic Numerical Diffusion in the LM.
- No. 4: Hans-Joachim Herzog, Ursula Schubert, Gerd Vogel, Adelheid Fiedler and Roswitha Kirchner (2002):
LLM - the High-Resolving Nonhydrostatic Simulation Model in the DWD-Project LITFASS. Part I: Modelling Technique and Simulation Method.
- No. 5: Jean-Marie Bettems (2002):
EUCOS Impact Study Using the Limited-Area Non-Hydrostatic NWP Model in Operational Use at MeteoSwiss.

- No. 6: Heinz-Werner Bitzer and Jürgen Steppeler (2004):
Description of the Z-Coordinate Dynamical Core of LM.
- No. 7: Hans-Joachim Herzog, Almut Gassmann (2005):
Lorenz- and Charney-Phillips vertical grid experimentation using a compressible nonhydrostatic toy-model relevant to the fast-mode part of the 'Lokal-Modell'
- No. 8: Chiara Marsigli, Andrea Montani, Tiziana Paccagnella, Davide Sacchetti, André Walser, Marco Arpagaus, Thomas Schumann (2005):
Evaluation of the Performance of the COSMO-LEPS System
- No. 9: Erdmann Heise, Bodo Ritter, Reinhold Schrodin (2006):
Operational Implementation of the Multilayer Soil Model
- No. 10: M.D. Tsyrlunikov (2007):
Is the particle filtering approach appropriate for meso-scale data assimilation?
- No. 11: Dmitrii V. Mironov (2008):
Parameterization of Lakes in Numerical Weather Prediction. Description of a Lake Model.
- No. 12: Adriano Raspanti (2009):
Final report on priority project VERSUS (VERification System Unified Survey).
- No. 13: Chiara Mirsigli (2009):
Final report on priority project SREPS (Short Range Ensemble Prediction System).
- No. 14: Michael Baldauf (2009):
COSMO Priority Project "Further Developments of the Runge-Kutta Time Integration Scheme" (RK); Final Report.
- No. 15: Silke Dierer (2009):
COSMO Priority Project "Further Developments of the Runge-Kutta Time Integration Scheme" (RK); Final Report.
- No. 16: Pierre Eckert (2009):
COSMO Priority Project "INTERP"; Final Report.
- No. 17: D. Leuenberger, M. Stoll, A. Roches (2010):
Description of some convective indices, implemented in the COSMO model.
- No. 18: Daniel Leuenberger (2010):
Statistical Analysis of high-resolution COSMO Ensemble forecasts, in view of Data Assimilation.
- No. 19: A. Montani, D. Cesari, C. Marsigli, T. Paccagnella (2010):
Seven years of activity in the field of mesoscale ensemble forecasting by the COSMO-LEPS system: main achievements and open challenges.
- No. 20: A. Roches, O. Fuhrer (2012):
Tracer module in the COSMO model.
- No. 21: M. Baldauf (2013):
A new fast-waves solver for the Runge-Kutta dynamical core.
- No. 22: C. Marsigli, T. Diomede, A. Montani, T. Paccagnella, P. Louka, F. Gofa, A. Corigliano (2013):
The CONSENS Priority Project.
- No. 23: M. Baldauf, O. Fuhrer, M. J. Kurowski, G. de Morsier, M. Muellner, Z. P. Piotrowski, B. Rosa, P. L. Vitagliano, D. Wojcik, M. Ziemianski (2013):
The COSMO Priority Project 'Conservative Dynamical Core' Final Report.
- No. 24: A. K. Miltenberger, A. Roches, S. Pfahl, H. Wernli (2014):
Online Trajectory Module in COSMO: A short user guide.
- No. 25: P. Khain, I. Carmona, A. Voudouri, E. Avgoustoglou, J.-M. Bettems, F. Grazzini (2015):
The Proof of the Parameters Calibration Method: CALMO Progress Report.

- No. 26: D. Mironov, E. Machulskaaya, B. Szintai, M. Raschendorfer, V. Perov, M. Chumakov, E. Avgoustoglou (2015):
The COSMO Priority Project 'UTCS' Final Report.
- No. 27: Jean-Marie Bettems (2015):
The COSMO Priority Project 'COLOBOC' Final Report.
- No. 28: Ulrich Blahak (2016):
RADAR_MIE_LM and RADAR_MIELIB - Calculation of Radar Reflectivity from Model Output.
- No. 29: M. Tsyrlunikov, D. Gayfulin (2016):
A Stochastic Pattern Generator for ensemble applications.
- No. 30: Dmitrii Mironov, Ekaterina Machulskaaya (2017):
A Turbulence Kinetic Energy - Scalar Variance Turbulence Parameterization Scheme.
- No. 31: P. Khain, I. Carmona, A. Voudouri, E. Avgoustoglou, J.-M. Bettems, F. Grazzini, P. Kaufmann (2017):
CALMO - Progress Report.
- No. 32: A. Voudouri, P. Khain, I. Carmona, E. Avgoustoglou, J.M. Bettems, F. Grazzini, O. Bellprat, P. Kaufmann and E. Bucchignani (2017):
Calibration of COSMO Model, Priority Project CALMO Final report.
- No. 33: Naim Vela (2017):
V.A.S.T. (Versus Additional Statistical Techniques) User Manual (v2.0).
- No. 34: C. Marsigli, D. Alferov, M. Arpagaus, E. Astakhova, R. Bonanno, G. Duniec, C. Gebhardt, W. Interewicz, N. Loglisci, A. Mazur, V. Maurer, A. Montani, A. Walser (2018):
COsmo Towards Ensembles at the Km-scale IN Our countries" (COTEKINO), Priority Project final report.
- No. 35: G. Rivin, I. Rozinkina, E. Astakhova, A. Montani, D. Alferov, M. Arpagaus, D. Blinov, A. Bundel, M. Chumakov, P. Eckert, A. Euripides, J. Foerstner, J. Helmert, E. Kazakova, A. Kirsanov, V. Kopeikin, E. Kukanova, D. Majewski, C. Marsigli, G. de Morsier, A. Muravev, T. Paccagnella, U. Schaettler, C. Schraff, M. Shatunova, A. Shcherbakov, P. Steiner, M. Zaichenko (2017):
The COSMO Priority Project CORSO Final Report.
- No. 36: A. Raspanti, A. Celozzi, A. Troisi, A. Vocino, R. Bove, F. Batignani(2018):
The COSMO Priority Project VERSUS2 Final Report
- No. 37: INSPECT Final Report A. Bundel, F. Gofa, D. Alferov, E. Astakhova, P. Baumann, D. Boucouvala, U. Damrath, P. Eckert, A. Kirsanov, X. Lapillonne, J. Linkowska, C. Marsigli, A. Montani, A. Muraviev, E. Oberto, M.S. Tesini, N. Vela, A. Wyszogrodzki, M. Zaichenko, A. Walser(2019):
The COSMO Priority Project INSPECT Final Report
- No. 38: G. Rivin, I. Rozinkina, E. Astakhova, A. Montani, J.-M. Bettems, D. Alferov, D. Blinov, P. Eckert, A. Euripides, J. Helmert, M.Shatunova(2019):
The COSMO Priority Project CORSO-A Final Report
- No. 39: C. Marsigli, D. Alferov, E. Astakhova, G. Duniec, D. Gayfulin, C. Gebhardt, W. Interewicz, N. Loglisci, F. Marcucci, A. Mazur, A. Montani, M. Tsyrlunikov, A. Walser (2019):
Studying perturbations for the representation of modeling uncertainties in Ensemble development (SPRED Priority Project): Final Report
- No. 40: E. Bucchignani, P. Mercogliano, V. Garbero, M. Milelli, M. Varentsov, I. Rozinkina, G. Rivin, D. Blinov, A. Kirsanov, H. Wouters, J.-P. Schulz, U. Schaettler (2019)
Analysis and Evaluation of TERRA_URB Scheme: PT AEVUS Final Report
- No. 41: X. Lapillonne, O. Fuhrer (2020)
Performance On Massively Parallel Architectures (POMPA): Final report
- No. 42: E. Avgoustoglou, A. Voudouri, I Carmona, E. Bucchignani, Y. Levy, J. -M. Bettems (2020)
A methodology towards the hierarchy of COSMO parameter calibration tests via the domain sensitivity over the Mediterranean area

- No. 43: H. Muskatel, U. Blahak, P. Khain, A. Shtivelman, M. Raschendorfer, M. Kohler, D. Rieger, O. Fuhrer, X. Lapillonne, G. Rivin, N. Chubarova, M. Shatunova, A. Poliukhov, A. Kirsanov, T. Andreadis, S. Gruber (2021)
The COSMO Priority Project T2(RC)2: Testing and Tuning of Revised Cloud Radiation Coupling, Final Report
- No. 44: M. Baldauf, D. Wojcik, F. Prill, D. Reinert, R. Dumitrache, A. Iriza, G. deMorsier, M. Shatunova, G. Zaengl, U. Schaettler (2021)
The COSMO Priority Project CDIC: Comparison of the dynamical cores of ICON and COSMO, Final Report
- No. 45: Marsigli C., Astakhova E., Duniec G., Fuezer L., Gayfulin D., Gebhardt C., Golino R., Heppelmann T., Interewicz W., Marcucci F., Mazur A., Sprengel M., Tsyrunikov M., Walser A.
The COSMO Priority Project APSU: Final Report
- No. 46: A. Iriza-Burca, F. Gofa, D. Boucouvala, T. Andreadis, J. Linkowska, P. Khain, A. Shtivelman, F. Batignani, A. Pauling, A. Kirsanov, T. Gastaldo, B. Maco, M. Bogdan, F. Fundel
The COSMO Priority Project CARMA: Common Area with Rfdbk/MEC Application Final Report